

Obscured pp -channel neutrino sources

Matthias Vereecken^{1,2} and Krijn D. de Vries¹

¹*IIHE/ELEM, Vrije Universiteit Brussel, Pleinlaan 2, 1050 Brussels, Belgium*

²*TENA, Vrije Universiteit Brussel, International Solvay institutes, Pleinlaan 2, 1050 Brussels, Belgium*

(Dated: February 10, 2022)

We explore the possibility that the astrophysical neutrinos are produced in pp -interactions with a gas cloud near the source acting as a beam dump, which is sufficiently dense to significantly attenuate the associated gamma-ray flux through pair-production on this gas. In this way, such sources could potentially supply the astrophysical neutrino flux whilst avoiding the existing constraints on the non-blazar contribution to the extragalactic gamma-ray background. After defining our model, we implement a Monte Carlo simulation and apply this to different scenarios. First, we investigate a set of active galaxies which exhibit signs of obscuration. We find that, currently, the expected neutrino flux from these objects in our model is below the existing exclusion limits, but can already constrain the amount of protons accelerated in such sources. Second, we investigate the diffuse neutrino flux generated by a population of obscured sources. We find that such a population can indeed alleviate the tension with the extragalactic background light. We discuss the possibility that ultra-luminous infrared galaxies represent such a source class.

Keywords: neutrino astronomy

I. INTRODUCTION

While the presence of a high-energy neutrino flux has been firmly established in recent years by the IceCube Neutrino Observatory, the sources of these neutrinos remain unknown. Recently, the first neutrino source has been identified: the flaring blazar TXS 0506+056. However, sources such as this one are unlikely to be responsible for the bulk of the observed diffuse neutrino flux [1, 2], although there is no consensus on this (see e.g. [3]). IceCube analyses show no significant clustering in either the high-energy starting events [4], which is a very pure sample at high energy, or the most recent all-sky point source searches using eight years of data [5], which includes events at lower energy, but has more contamination by background.

The results from the all-sky clustering search indicate that the total diffuse flux is not dominated by a few individually powerful sources. However, it could still be dominated by a single source class, with blazars and gamma-ray bursts standing out as candidate sources, since they are rare and powerful enough to be well-detectable. Stacked searches for neutrinos from blazars [6, 7], selected for their bright (gamma-ray) emission, has limited the contribution of these blazars to a few percent up to $\sim 30\%$ of the diffuse neutrino flux, depending on the energy range and spectral index of the emitted neutrinos. Similarly, searches for neutrinos from gamma-ray burst in their prompt phase [8], find results compatible with background, limiting the total contribution from such events to $\leq 1\%$.

Despite these null-results, it is possible to infer some general properties of the neutrino source population by combining the non-detection of such a population with the requirement that the sources still need to supply the detected astrophysical flux [9–14]. Each individual neutrino source needs to have a low neutrino luminosity in

order to not have shown up in any point source search. On the other hand, this means that the population needs to be sufficiently numerous in order to supply the detected astrophysical neutrino flux. These constraints already disfavour several important source classes as the (dominant) source of the observed astrophysical neutrinos, such as BL Lacs and standard FSRQ scenarios.

In addition to direct searches, possible neutrino sources are also strongly constrained by measurements of the (diffuse) gamma-ray flux, since neutrinos and gamma rays are produced together in proton-photon or proton-proton interactions. A priori, one can use the extragalactic gamma-ray background (EGB) for this, since it is the total gamma-ray flux from outside our galaxy. However, tighter constraints can be achieved by subtracting known sources of gamma rays that do not contribute to the neutrino flux. Most of the EGB flux is due to blazars, whose spectra can typically be explained with leptonic emission only and whose total neutrino emission is constrained. Therefore, the gamma-ray flux associated to neutrino emission can instead be compared with the unresolved gamma-ray flux, the isotropic diffuse gamma-ray background (IGRB). Alternatively, one can also compare with the estimated (i.e. model-dependent) non-blazar contribution to the EGB, which attempts to also subtract unresolved blazars from the diffuse flux.

The comparison between the diffuse neutrino and gamma-ray fluxes gives very important constraints in the case of CR reservoir models, which feature pp -interactions. In such models, cosmic rays are confined in e.g. a starburst galaxy or galaxy cluster, such that the interaction probability becomes appreciable after integrating over the cosmic ray path length, while the produced gamma rays and neutrinos can escape unhindered. Earlier studies for pp -sources in general [15] and for star-forming galaxies in particular [16] found that the neutrino flux observed by IceCube was compatible with the

observed gamma-ray background for spectral indices α around ~ 2.1 . Later studies, however, disfavour star-forming galaxies as the dominant source of neutrinos [17]. Using stronger constraints from the bound on the non-blazar contribution to the EGB, which is about 28% [18–24], it is difficult to explain the neutrino flux without simultaneously violating this bound on the gamma-ray flux. This is due to the combination of two effects. First, the gamma-ray spectrum produced in pp -interaction goes down to low energy (since the energy required to for proton-proton interaction is almost trivially satisfied in the centre-of-mass frame). Second, during propagation, high-energy gamma rays initiate an electromagnetic cascade by interacting with the cosmic microwave background and extragalactic background light. Consequently, there is a build-up of lower-energy gamma rays in the 1–100 GeV band observed by Fermi-LAT [25, 26]. As a result, the diffuse gamma-ray flux in this band violates the existing bounds. More recently, however, a study of hadronically powered gamma-ray galaxies [27], such as starbursts and ultra-luminous infrared galaxies, finds instead that a spectral index $\alpha < 2.12$ is still compatible with all observations, including the most recent estimates of the non-blazar contribution to the EGB.

In $p\gamma$ -source scenarios, there is a lower limit on the energy of the produced gamma-rays from π^0 -decay, such that their flux at lower energies, i.e. in the Fermi band, is only generated through the electromagnetic cascade. Therefore, the constraint from the above argument is slightly weaker (although dependent on specific models for the target radiation field). Still, given that the non-blazar contribution to the EGB is already constrained below 28% and bright gamma-ray blazars detected by Fermi are disfavoured as the main source of the neutrinos, a tension remains when considering the gamma-ray flux produced by $p\gamma$ -neutrino sources. This tension can be resolved when considering photon-photon annihilation inside these sources, caused by the same radiation field as the one responsible for $p\gamma$ -interactions. As shown in [28], $p\gamma$ -neutrino sources bright in X-rays or MeV gamma-rays (assuming these can escape the system unhindered) can be such sources. As a result of the many constraints above, conventional sources like gamma-ray bursts and active galactic nuclei bright in gamma rays are unlikely to form the dominant contribution to the diffuse neutrino flux. Instead, neutrino sources are likely dim in GeV gamma rays [28].

In this context, we investigate a model of neutrino sources which are obscured in gamma rays, as well as X-rays, by a dense gas cloud with column density $N_H^{(1)} = 5 \times 10^{25} \text{ cm}^{-2}$ or $N_H^{(2)} = 10^{26} \text{ cm}^{-2}$ close to the source. We envision a scenario where this dense gas gets bombarded by accelerated cosmic rays, acting as a beam dump. Such a scenario was first considered in [29]. We develop a Monte Carlo code to calculate the predicted neutrino and gamma-ray fluxes from such a scenario.

We apply our model first to a selection of active galaxies which are possibly obscured. We compare our predic-

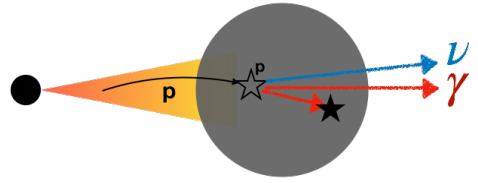


FIG. 1: Schematic representation of the model we consider for neutrino and gamma-ray production from pp -interactions of cosmic rays with a dense gas cloud near the cosmic-ray source acting as a beam dump. Due to the high integrated column density of the gas cloud, the produced gamma rays are also attenuated by the same cloud through Bethe-Heitler pair production. The relative size of the cloud and the source/outflow can vary. Note that while the figure features a jet, this is not a requirement for this mechanism to work and we do not initially assume its existence in our calculations.

tion with current constraints from IceCube and put constraints on the possible proton content of these sources under our model. Afterwards, we calculate the diffuse neutrino and gamma-ray fluxes from a population of obscured sources to investigate whether such a population of sources can explain the diffuse neutrino flux without exceeding the measured extragalactic gamma-ray background in our model. We find that our model indeed alleviates the tension. In this context, we also consider in more detail ultra-luminous infrared galaxies as a promising source category.

II. NEUTRINOS FROM OBSCURED pp -SOURCES

In this section, we introduce our model for obscured pp -sources, discuss the properties of the gas cloud and the attenuation of gamma rays near the source.

A. Model definition

In our model, we consider the setup shown schematically in Figure 1. A source of accelerated cosmic rays is obscured from our line of sight by a sufficiently large and dense cloud of gas near to the source, which acts as a beam dump for accelerated cosmic rays. The cosmic rays interact hadronically with the gas in pp , pA , or AA -interactions, although we will only consider pp -interactions. In these interactions, neutrinos and gamma rays are produced. The gas cloud is sufficiently thick that the gamma rays can interact again with the remaining part of the gas column after their production, undergoing Bethe-Heitler pair production [30]. Therefore, the source can be hidden (or at the very least obscured) in gamma rays.

The amount of matter present in the gas cloud is expressed by the equivalent hydrogen column density N_H , defined as the line-of-sight integral of the hydrogen den-

sity n_H

$$N_H = \int dl n_H(l), \quad (1)$$

and denotes the amount of hydrogen atoms per cm^2 . The column density required for the gamma-ray attenuation at GeV energies and above to be significant can be estimated from the Bethe-Heitler pair production cross section with matter. Using the approximate value $\sigma_{\text{BH}} \approx 20 \text{ mb} = 2 \times 10^{-26} \text{ cm}^2$, we see that we require a column density of approximately

$$N_H = 5 \times 10^{25} \text{ cm}^{-2}. \quad (2)$$

While such a column density is rather high, we will motivate its use in Section II C. In this work, we explore the possibility that neutrinos are produced in highly obscured sources, investigating two benchmark values of the column density: $N_H^{(1)} = 5 \times 10^{25} \text{ cm}^{-2}$, which is easily motivated, or the higher value $N_H^{(2)} = 10^{26} \text{ cm}^{-2}$.

As a consequence of this high column density, (nearly) all cosmic rays will interact with the gas before traversing the cloud, since the proton-proton cross section σ_{pp} (starting at $\sim 30 \text{ mb}$ and rising with energy, see e.g. the analytic expression in [31]) is a few times higher than the Bethe-Heitler pair production cross section σ_{BH} . Therefore, such a neutrino source would be a poor cosmic ray source, although similar but unobscured sources would still make excellent cosmic ray sources. The remaining gas column after interaction is sufficiently thick for secondary protons to interact with the cloud again, giving a slight boost to the total neutrino and gamma-ray flux, although this contribution will turn out to be negligible.

While the sketch in Figure 1 shows an AGN-like scenario featuring a jet, and we will apply the model to objects of this scale, the mechanism is not restricted to this case and we do not a priori assume the existence of a jet in our calculations. The only requirement is that there exists a compact source of accelerated cosmic rays obscured by a dense gas cloud near to the source. In principle, such a model can feature both transient and continuous neutrino production, although we restrict ourselves to continuous emission and assume that the configuration is stable for a sufficiently long time, where “sufficiently long” depends on the specific case under consideration.

The beam dump model considered here should be contrasted with cosmic ray reservoir models of neutrino production. There, cosmic rays have a significant interaction probability with the target gas only by integrating the gas density over the cosmic ray trajectory inside a galaxy or cluster, since cosmic rays are confined in these structures. Gamma rays, which are not confined, escape unattenuated. Instead, in our model discussed here, the interaction happens close to the source with a thin, but dense target (i.e. the cosmic rays are not confined to this region), such that the cosmic rays and gamma rays traverse the same gas column. On the other hand, cosmic ray accelerator models with a similar configuration

(e.g. [32, 33]) typically feature lower column densities, such that the gamma ray flux is either unattenuated or attenuated only by invoking a strong radiation field.

Another model with more similarities to our scenario but of a different scale is one of the microquasar SS433, where a supergiant star feeds a $10 M_\odot$ black hole [34–36]. Inside the jet, accelerated particles undergo pp -interactions with cold matter and produce both neutrinos and gamma rays. In this model, attenuation of gamma rays by both Bethe-Heitler pair production and photomeson production are taken into account, on top of the more standard $\gamma\gamma$ -annihilation.

Typical neutrino models consider sources from which strong non-thermal emission, usually X-ray or gamma ray, has been observed. Instead, our model features objects with obscured gamma- and X-ray emission. Therefore, strong sources can only be selected at radio or infrared wavelengths, where the presence of an accelerated particle population can also be inferred. The phenomenology of our model also differs from that of the hidden sources in [28], where strong X-ray emission is required in order to attenuate the gamma rays.

B. Cloud dynamics

As already mentioned, often our source will feature a jet which is impacting the gas cloud. While we assume that this configuration is stable for a sufficiently long time, either on the observing timescale or a relevant period in the cosmological history of the source, eventually such a jet will break up the configuration if it is sufficiently strong at the location of the cloud. The exact physics depends on the location of the cloud, its total mass and the strength of the jet. A full study of this is outside the scope of this work. However, similar studies exist in the literature, which we briefly discuss here.

The interaction of a cloud of cold gas with a jet¹ was studied in [37, 38]. Due to the pressure of the jet, some or all of the cloud material can be blown away and swept up by the jet. Initially, the interaction will cause shocks in both the jet and cloud material, which can serve as a potential site for particle acceleration. As the material is swept up by the jet, eventually it will spread out and move along with the jet, at which point significant interactions between the cloud and jet cease. Depending on the kinetic energy of the jet and the mass of the cloud, the jet might be slowed down.

Several scenarios have been studied in the literature, often with a cloud or a star interacting with an AGN jet. Due to the scale of the cloud/star compared to the jet (i.e. typically much smaller than the jet at entry),

¹ Note that the jet and cloud have different properties: a jet is a Poynting flux (i.e. dominated by radiation) or extremely relativistic matter, while a gas cloud is dense and cold matter.

these scenarios feature transient emission and have been invoked to explain gamma-ray flares in blazars [38, 39]. These models differ from the scenario we envision mostly due to the scale of the cloud, since we focus on a case where a possible jet is obscured for an extended amount of time².

Jet-cloud/star models have been used to explain the neutrinos from the blazar TXS 0506+056. The bright gamma-ray flare associated with a high-energy neutrino has been modelled using clouds with $N_H > 10^{24} \text{ cm}^{-2}$ present in the broad-line region of the blazar [41]. The electromagnetic cascade initiated by the pp -interactions (modelled using the analytical fits to the kinematic distributions of final state particles) ionises the cloud, which becomes optically thick for optical to X-ray photons while the gamma rays and the neutrinos escape. The SED at lower frequencies can then be explained with a second leptonic emission zone. This scenario can explain the observed neutrino and electromagnetic emission with moderate proton luminosity, in contrast with $p\gamma$ -models which have a low interaction rate in order to avoid efficient $\gamma\gamma$ -annihilation and therefore require high proton luminosity. The neutrino flare during the quiescent state of the blazar has been explained with unbound layers from a tidally-disrupted red giant³ [43]. In this case, the target has a column density of $N_H = 5 \times 10^{25} \text{ cm}^{-2}$, the same as our first benchmark point. Again, the cloud becomes ionised and is optically thick to X-rays, but now the Comptonised radiation field is also sufficiently thick to efficiently attenuate gamma rays through $\gamma\gamma$ -pair production.

There are additional models featuring jet-cloud/star interactions built only to explain gamma-ray emission. A model of jets interacting with a BLR cloud of lower density than those above was investigated in [44]. In [45], particle acceleration is induced by a strong star wind and loss of mass of a star in an FSRQ jet. Another study investigates M87 TeV flares from jet-cloud interaction which accelerates particles and leads to pp -interactions [42]. Finally, in an alternative scenario for orphan flares, such flares are caused by the interaction of accelerated particles with star radiation inside jet blobs [46].

C. High column densities

The column densities required for the gamma-ray attenuation to be significant are high compared to typical astrophysical environments. The average column density

of our own galaxy is $N_H^{\text{gal}} \sim 10^{20} \text{ cm}^{-2}$, driven mainly by the interstellar medium and not the compact objects (stars) within. On the other hand, Earth's atmosphere has a column density of 10^3 g cm^{-2} or $N_H \sim 10^{26} \text{ cm}^{-2}$, similar to the column density we are considering. Still, the latter is a compact object and thus not a good comparison for the viability of our scenario, although it is more appropriate as a comparison for the jet-cloud/star scenario. In order to have longer lasting neutrino production and obscuration, a more extended gas cloud is necessary.

Though rare, astrophysical environments with a gas column of the required magnitude do exist. As already mentioned in the previous section, models of AGN jets interacting with dense clouds possessing column densities up to $5 \times 10^{25} \text{ cm}^{-2}$ have been invoked to explain the TXS 0506+056 neutrino and gamma-ray flares. More generally, supermassive black hole in AGNs are surrounded by gas and dust in the broad-line region and torus (for a review, see [47, 48]). In case an AGN is observed edge-on, the central engine is frequently hidden from our view by the dusty torus. The column density of this torus varies and an AGN is generally considered obscured when $N_H \geq 10^{22} \text{ cm}^{-2}$. Below $N_H \sim 10^{24} \text{ cm}^{-2}$, the photon attenuation cross section in the 2–10 keV X-ray regime has the correct magnitude to probe this column density⁴. If the column density is higher than the inverse of the Thompson cross section, $N_H \geq 1.5 \times 10^{24} \text{ cm}^{-2}$, the AGN is called Compton-thick [49]. At these values, the density can be probed by hard X-rays ($E_{\text{X-ray}} \geq 10 \text{ keV}$), where Compton scattering dominates. However, for densities above $N_H = 10^{25} \text{ cm}^{-2}$ (heavily Compton-thick), the X-ray emission is suppressed even above 10 keV, since the photons are down-scattered by Compton interactions and subsequently absorbed. Other (indirect) methods need to be used to probe these obscuring columns (e.g. through reflected X-rays). In this way, Compton-thick AGNs have been found with column densities exceeding $N_H = 10^{25} \text{ cm}^{-2}$ [49, 50]. AGNs obscured by column densities significantly higher than 10^{25} cm^{-2} are suspiciously missing from surveys. From the above discussion, it is clear that there is an observational bias against such highly obscured objects.

The Chandra X-ray Observatory [51] detects X-rays between 0.1–10 keV and has been used to detect obscured AGNs. An analysis fitting AGN spectra in Chandra Deep Fields with physical models, finds many highly obscured AGNs [52]. While their analysis corrects for observational bias, they are unable to constrain the number of AGNs with $N_H \geq 10^{25} \text{ cm}^{-2}$, since these sources are missed in their sample and therefore the missing number

² In this sense, our model has some similarities with low-luminosity gamma-ray burst models, where the jet is stopped by a cocoon of matter [40].

³ A red giant is necessary since only there the outer layers are sufficiently weakly bound to be blown away and interact with a significant portion of the jet [42].

⁴ More specifically, the main indicator is the photo-electric cut-off, induced by the sharply rising cross section of photo-electric absorption towards low energies.

of sources cannot be determined. As such, sources of this kind may contribute to the heavily obscured AGN population. This agrees with earlier results presented in [53]. Other analyses do find multiple objects with $N_H \geq 10^{25} \text{ cm}^{-2}$, even up to $N_H \sim 10^{26} \text{ cm}^{-2}$ in Chandra surveys [54]. Another analysis studies torus model properties [55] with an ultra-hard X-ray sample (14–195 keV) of Seyfert galaxies from Swift/BAT [56], which can identify more strongly obscured objects. They find that even from such a selection, a population of the most obscured objects is still missing, agreeing with [50, 57, 58].

An example of such an obscured source is NGC 4418, a luminous infrared galaxy (LIRG). It has a core bright in IR along with the deepest known silicate absorption, but it has not been detected in X-rays [55, 59]. Its inferred column density is $N_H > 10^{25} \text{ cm}^{-2}$, with a spectrum consistent with AGNs as the main power source and showing similarities with ARP 220 [60] (which will end up as a source in the analysis of Section IV). Another analysis finds that an AGN is only allowed in case the column density exceeds this same value [61].

While the objects above do have strong obscuration, this does not yet mean that the obscuring material is bombarded by cosmic rays or blocks a jet. However, there exist several models of tilted tori that envision such a scenario [47, 62]. We show that such configurations provide interesting sites for neutrino production through the model proposed in this paper.

It follows that, while extreme, column densities $N_H > 10^{25} \text{ cm}^{-2}$ in astrophysical environments are very likely to occur. Therefore, our lower benchmark value $N_H^{(1)} = 5 \times 10^{25} \text{ cm}^{-2}$ for obscured neutrino sources is compatible with the conventional view of various astrophysical objects. On the other hand, values much higher than this have not been observed, such that we consider our second benchmark $N_H^{(2)} = 10^{26} \text{ cm}^{-2}$ as a more extreme, but still realistic, case.

D. Photon attenuation

In this section, we discuss the attenuation of photons at the source, in particular X-rays and gamma rays, since photons at these energies are sensitive to the presence of surrounding matter and their appearance is linked to high-energy particle acceleration and interactions. Since attenuation can be both due to matter and radiation, we discuss these separately.

1. Attenuation by matter

The interaction of X-rays and gamma rays with matter, which is the main attenuation channel in our model, happens through different processes. The photo-electric effect is important for soft X-rays traversing an unionised medium. For hard X-rays propagating through any medium, Compton scattering is important. Finally, for

gamma rays, Compton scattering dominates at MeV energies, while at GeV energies pair production on either the electrons or the nuclei is dominant. The strength of these interactions depends on the energy of the photons and the target composition. For GeV gamma rays, which will be considered in this work⁵, the only relevant process is pair production, either on the nuclei or on electrons.

The target gas is expected to have a composition similar to the interstellar medium, which is dominated by hydrogen [64]. The hydrogen equivalent column density reported by astronomers, derived from spectral modelling, takes this composition into account. The total amount of matter in the column is then given by summing over all elements, with a density equal to N_H times the abundance a_Z of that element relative to hydrogen

$$N = \sum_Z a_Z N_H, \quad (3)$$

see e.g. [65], and the absorption models included in XSPEC [63]. However, given the dominance of hydrogen, we assume that the target is a pure proton gas when considering the interactions with accelerated particles⁶. For modelling the X-ray attenuation, this introduces a rather large error, since both photo-electric absorption and Compton scattering are strongly dependent on the target element. For our model, however, where we are mainly interested in the gamma-ray attenuation, this is a reasonable assumption, which we explicitly checked using attenuation cross sections retrieved from the XCOM database [67].

The gamma-ray attenuation is dominated by Bethe-Heitler pair production [30], the expression for which can be given as a series expansion in [68] (see also the review [69] and an earlier treatment in [70]). The threshold for pair production is $E_{\text{BH}}^{\text{thres.}} = 2m_e c^2$. For the full pair production cross section $\sigma_{\text{BH}}(E_\gamma)$ (on proton *and* electron), we use this expression multiplied by 2. Since the cross section rises only logarithmically with the photon energy, the cross section is approximately constant with a value of $\sigma_{\text{BH}} \approx 20 \text{ mb}$. This validates our estimation of the required column density N_H in Eq. (2).

For cross-section gamma rays in matter, the interaction cross section with matter starts to decrease due to the ‘‘Landau-Pomeranchuk-Migdal’’ (LPM) effect [71–75] (see also the PDG review [76]). This effect is due to destructive interference between amplitudes from different, nearby, scattering centres. However, for an astrophysi-

⁵ In order to properly model X-rays propagating through a medium with Compton scattering, multiple scattering needs to be taken into account, in particular when the densities are high. This requires the use of specialised codes, such as XSPEC [63].

⁶ For neutrino and gamma-ray production, the additional mass (increase by a factor of ~ 1.4) due to the heavier elements can be included by rescaling N_H , see for example [33, 66]. However, for the purpose of our work, we do not explicitly take into account this small numerical factor.

cal gas cloud, the density is too low for this effect to be relevant, even if the integrated column density is high.

Another possible source of gamma-ray attenuation would be through photohadronic $p\gamma$ -interactions. However, the cross section for this process is much lower than for pair production⁷ and we will therefore neglect it (see also the related discussion in Section II E).

2. Attenuation by a radiation field

Gamma rays can also interact with a radiation field at the source and undergo pair production if the centre of mass energy exceeds $2m_e$, attenuating the gamma-ray flux. The optical depth to pair production depends on the number density of photons (i.e. the energy density of the radiation field). We can ignore this attenuation channel if the radiation fields at the cloud are weak enough for $\gamma\gamma$ -pair production. In case of a strongly radiating source (as will usually be the case), this means that the cloud can not be too close to the source. Otherwise, pair production on radiation will further decrease the gamma-ray flux.

Even if there is not a sufficiently strong radiation field present at first, it can be generated by the particle cascade initiated in the pp -interactions. Depending on the density and location of the gas cloud, the gamma rays and e^\pm -pairs produced in pion decay can initiate an electromagnetic cascade through repeated creation of photons through synchrotron radiation, bremsstrahlung, and inverse-Compton scattering and the creation of e^\pm -pairs through pair production. As a result, the cloud can become fully ionised and the photon field can become Comptonised. The cloud is then optically thick to X-rays (due to the free electrons) and the generated photon field can act as a target for gamma-ray pair production (see e.g. [43]), decreasing the gamma-ray flux.

Since $\gamma\gamma$ -attenuation introduces a stronger model dependency, we do not take this additional attenuation channel into account. In that sense, the amount of gamma-ray obscuration we obtain in our model is conservative.

E. Model assumptions

In addition to intrinsic features of our model, we also make some further assumptions in order to reduce the parameter space. The cosmic-ray composition is considered to be pure proton, which is a reasonable approximation in the energy range relevant for IceCube. As already mentioned in Section II D, the target gas is approximated as

pure hydrogen. Therefore, we can model the interactions as pure pp -collisions, without complications from nuclear effects.

We do not include additional sources of neutrinos or gamma rays, i.e. $p\gamma$ -interactions and leptonic processes, since these are highly model dependent. Typically, $p\gamma$ -interaction models require higher proton luminosities than pp -models to obtain sizeable fluxes⁸. Therefore, if pp -interactions are present, they can be expected to be dominant compared to $p\gamma$ -interactions. Additional gamma rays can be produced in leptonic processes, such as through inverse-Compton scattering. Both $p\gamma$ -interactions and leptonic processes increase the total gamma-ray flux. This increase is counterbalanced by attenuation through $\gamma\gamma$ -pair production on the intense radiation fields present inside the cloud (which we do not take into account), reducing the total gamma-ray flux. In addition, if the latter process is not dominant, it is safe to ignore photomeson production, since its interaction rate is roughly three orders of magnitude smaller than $\gamma\gamma$ -annihilation for the same photon field [28, 41, 77].

We do not take into account synchrotron losses of the muons, pions and kaons. However, for the scenario we envision, these losses should be negligible: while the obscuring gas should be close to the source, it can not be too close, otherwise we need to take into account the effect of strong radiation fields on the gas. Therefore, if the gas is sufficiently far removed from the source, one can expect the synchrotron losses due to the magnetic fields to be negligible. Indeed, following the approach of [78], we can estimate above which critical energy these losses become dominant (i.e. the timescale associated to synchrotron losses is shorter than the decay time), for an AGN jet scenario with the gas cloud at parsec scales. We find that this energy can easily exceed 10^6 GeV even for the magnetic fields associated to jets, using the magnetic fields found in [79] or higher; if no (strong) jet is present at the location of the cloud, magnetic fields are expected to be even weaker at the parsec scale.

Unless otherwise stated, the protons are assumed to follow an E^{-2} -spectrum, consistent with Fermi acceleration. However, this immediately implies that the predicted neutrino spectrum also follows an E^{-2} -spectrum, while IceCube observes a softer spectrum [4]. Therefore, the computation here can only serve to explain the observed neutrino flux above ~ 100 TeV, while there must be a second, softer, component below this energy that we do not model.

With these assumptions and the choice of two benchmark values of N_H , the only free parameters left are the normalisation of the injected proton flux (used in Section IV) or the resulting neutrino or gamma-ray flux

⁷ This is the reason that $p\gamma$ -interaction models require strong radiation fields (leading to gamma-ray attenuation) and much larger proton luminosities than pp -interaction models.

⁸ This is due to their much lower cross section, which might not be compensated completely by the high target density of a radiation field

(used in Section V) and the energy range in which the protons are injected. The maximum energy of the protons will be fixed at 10^8 GeV, which is sufficient to explain the neutrinos observed by IceCube without violating the limits at the highest energy. The minimum proton energy is determined by the acceleration mechanism. In the case of shock acceleration, one typically has $E_p^{\min} \sim \Gamma m_p c^2$ [80], with Γ the Lorentz factor of the shock, which is the minimum energy with which the particles can efficiently participate in the acceleration process. Sometimes, also the value $E_p^{\min} \sim \Gamma^2 m_p c^2$ is used [28]. Since we will consider AGNs as the central engine in the following, with $\Gamma \sim 10 - 30$ [81], we take $E_p^{\min} = 10^2$ GeV. For an E^{-2} -spectrum, the final result is not very sensitive to the exact value of the minimum energy (as long as it is around the same order of magnitude), since the luminosity in this case is divided equal per decade of energy. More concretely, we have

$$L \propto \int_{E_{\min}}^{E_{\max}} dE E E^{-2} = \ln \left(\frac{E_{\max}}{E_{\min}} \right), \quad (4)$$

resulting in only a logarithmic dependence on the minimum energy. Nevertheless, varying the minimum energy with more than an order of magnitude has a significant effect on the total normalisation of the flux. More importantly, if the spectral index deviates from 2, the luminosity quickly becomes very sensitive to the minimum energy, see also the discussion in [82] and Section IV B. Since cosmic ray experiments are only sensitive to the maximum energy of extragalactic cosmic rays (below the knee galactic cosmic rays dominate), this is an important source of uncertainty. However, the choice we make above is theoretically well motivated.

III. CALCULATING THE ν AND γ -RAY FLUX

In this section, we describe the method for calculating the neutrino and gamma-ray flux for our model of neutrino production in obscured sources, before applying it to specific scenarios in the following sections. We perform the calculation in two ways. For the first one, we use analytical fits of the neutrino and gamma-ray spectrum from pp -collisions. For the second one, we use a full Monte Carlo simulation for the pp -interactions. For our final results, we use the Monte Carlo simulation, since it includes more details, while the analytical method serves only as a consistency check on our results.

The analytical calculation of neutrino and gamma-ray spectra from cosmic ray interactions with a cloud of integrated column density N_H follows the method of [31]. These authors provided analytical fits to the neutrino and gamma-ray spectra using the meson spectra simulated with the Monte Carlo generators SIBYLL [83] and QGSJET [84], with their subsequent decay to photons, neutrinos and electrons treated analytically. Note that using these fits, we have no access to the secondary proton

spectrum and therefore can not implement the interactions of secondary protons. For simplicity, and because this calculation serves only as a sanity check, we implement the gamma-ray attenuation using the full column density of the cloud, ignoring that the gamma rays are created somewhere along the column and do not see the entire gas column.

These analytical fits are accurate and faster than performing Monte Carlo simulations. Nevertheless, a full Monte Carlo simulation was performed in order to model the neutrino production in more detail. The two main reasons are that this allows us to use an updated Monte Carlo generator for performing the pp -interactions and that in this way we have access to secondary protons, which can interact again with the gas column. We implemented our model with the Monte Carlo generator SIBYLL 2.3 [85], which is an updated version of the code used for the analytical fits above. In particular, it includes the contribution from charmed meson decay [86, 87], although this does not noticeably impact our results⁹.

In the simulation, protons are propagated through a matter column of specified integrated density N_H and allowed to interact using standard Monte Carlo techniques¹⁰. Initially, in order to build up sufficient statistics at high energies, we inject a proton with an energy which is drawn from a power law distribution following E^{-1} . Afterwards, events are reweighted to the distribution under study ($\propto E_p^{-2}$ unless otherwise stated).

The mean free path of a proton of energy E_p under pp -interactions propagating through a medium with density n is given by

$$\lambda(E) = \frac{1}{n\sigma(E_p)}, \quad (5)$$

which is determined using the cross section tables calculated by SIBYLL. The interaction point of a proton can be determined by sampling from the distribution

$$P(n_r < n_\lambda) = 1 - e^{-n_\lambda}. \quad (6)$$

If this point is beyond the total depth of the gas column at the respective proton energy $n_{\lambda, \text{tot}}(E_p) = N_H \sigma(E_p)$, the proton escapes and is saved in the final output. Otherwise, a collision is performed using SIBYLL and the final state particles ν_α , $\bar{\nu}_\alpha$, e^\pm and γ are saved, while

⁹ This is in contrast with the result for atmospheric neutrinos, where charmed meson decay produces a distinct, harder spectrum. However, the reason for this difference is that in atmospheric neutrino production there is a competition between the decay of the meson and its interaction with an air nucleus. The latter produces softer spectra, since it initiates a new cascade. Because charmed mesons have a shorter lifetime, their contribution produces a harder spectrum. In astrophysical scenarios, this competition is not present, as also mentioned in [32].

¹⁰ See e.g. the GEANT4 [88] physics reference manual.

secondary p , n and their antiparticles are allowed to interact again with the remaining column¹¹. These secondary interactions have a minor effect. This is a simple consequence of the power law proton spectrum: the N secondary protons produced by a proton of energy E_p carry on average a fraction x of the parent proton energy and are dominated by the primary protons at the lower energy xE_p , which are more numerous by a factor $\frac{(xE_p)^{-2}}{NE_p^{-2}} = \frac{1}{x^2N}$. Since the sum of all secondary energies (including leptons and gamma rays) needs to total E_p , we have $xN < 1$ and $x < 1$, so the primary protons are indeed dominant.

The decay of pions and other mesons to neutrinos is performed by the SIBYLL decay routines. In order to obtain a better accuracy, these decay routines are often replaced by analytical calculations or by interfacing the output to other codes like `Pythia` [89]. However, these inaccuracies are mainly important for air shower simulations, where the full particle spectrum of individual events needs to be well modelled. For our purposes, where we only care about the total neutrino spectrum, the SIBYLL routines should suffice. Neutrons are considered stable in this simulation (the additional neutrinos from their decay outside of the source are at low energy, since most of the energy goes towards to resulting proton).

The attenuation of photons, taking into account only the remaining gas column, is taken into account by reweighting each photon by¹²

$$w_\gamma(E_\gamma, E_p) = e^{-N_H \sigma_{\text{BH}}(E_\gamma) \left(1 - \frac{n_\lambda}{n_{\lambda, \text{tot}}(E_p)}\right)}, \quad (7)$$

where n_λ is the number of mean free paths the proton travelled before interacting (i.e. where the photon is produced) and $n_{\lambda, \text{tot}}(E_p)$ is the total number of proton mean free paths of the cloud for the energy of the parent proton.

Finally, the overall normalisation of the produced spectra is determined in different ways, depending on the scenario under consideration.

¹¹ For simplicity, the cross section of interactions with protons is put equal to the proton-proton cross section for all these particles (i.e. also for n and anti- p/n), which is a good approximation at high energies.

¹² Note that by using this formula, we implicitly reduce the simulation to a one-dimensional one, ignoring the photon momentum in the direction perpendicular to the initial proton direction. While taking this into account would increase the gas column seen by the photon in the case of an infinite “plane” of gas, this correction is minor due to the beaming. Moreover, taking into account a more realistic geometry than a flat infinite plane would decrease the column slightly.

IV. OBSCURED FLAT-SPECTRUM RADIO AGNS

In this section, our model is applied to a set of AGNs selected for their possible obscuration by matter. We first review the object selection [29] which we use. Next, we discuss our normalisation, based on the measured radio flux from these AGN. Finally, we show the results and, using existing limits on their neutrino emission from IceCube [7], derive limits on the cosmic ray content of these sources.

The original motivation for this object selection is the possibility of having AGNs with tilted tori [47, 62]. In this case, the jet can penetrate the dust torus, which has a considerable integrated column density, and produce neutrinos efficiently while being obscured in X-rays. However, the exact origin of the gas cloud is not important for the details of our calculation. We assume the cloud is stable on observation timescales (i.e. at least years). Due to the strong electromagnetic radiation from the jet, the cloud becomes ionised [29]. At the same time, these radiation fields also attenuate the gamma rays through $\gamma\gamma$ pair production, which we do not model. The gamma ray flux predicted is therefore an upper limit on the hadronic gamma rays. On the other hand, leptonic processes might create additional gamma rays. However, for this application, we are only interested in the neutrino emission from these objects and do not model their complete SED.

A. Selected objects

We investigate the obscured flat-spectrum radio AGN selected in [29], which targets nearby sources which are candidate cosmic ray accelerators, feature beamed emission (i.e. a jet, so that all emission is boosted towards Earth) and which exhibit signs of obscuration by matter by selecting those objects with a lower-than-expected X-ray luminosity, relative to the radio luminosity. Whereas X-rays are hindered by gas, radio waves can propagate through gas unimpeded. Moreover, radio emission is usually explained by synchrotron emission from a non-thermal population of electrons. Therefore, the radio emission from these sources characterises the strength of the inner engine. Under the assumption that the reduced X-ray emission relative to the radio emission is (mainly) due to attenuation by matter, these objects are potential strong neutrino sources through pp -interactions (in addition to the $p\gamma$ -interactions, which we ignore).

The study in [29] first considers an unbiased set of nearby cosmic ray source candidates which exhibit signs of beamed emission towards Earth. Assuming that their original set consists of generic sources and that the observed spread in X-ray intensity relative to the radio intensity is due to the presence of gas and dust, they select the 25% weakest sources as heavily obscured, retaining 15 objects.

In order to estimate the fraction of interacting protons from the X-ray obscuration, we need to know the column density of the obscuring matter. This can be determined from the observed X-ray flux if we know which process is responsible for X-ray attenuation. At higher X-ray energies, this is always Compton scattering (which we already discussed in Section IID), but at 1.24 keV photo-electric absorption dominates if the electrons are still bound in atoms. Due to the strong radiation of these sources, however, the obscuring gas cloud is completely ionised for natural geometries. Indeed, following the analysis in [29], for natural values of the cloud thickness and distance from the central engine, i.e. between 1 and 10 pc, and for typical values of AGN luminosity and ionisation, the cloud will be fully ionised due to Compton scattering. In this case, the column density leading to an obscuration in X-rays of $\sim 90\%$ is $N_H \sim 10^{26} \text{ cm}^{-2}$. This also corresponds to the required column density for significant neutrino production to occur, since Compton scattering on hydrogen and proton-proton interactions have a similar interaction cross section. Using the Compton scattering cross section, the fraction of interacting protons derived in [29] for the objects in the selection above varies between 0.80 and 0.99, which corresponds to column densities $N_H \sim 5 \times 10^{25} - 10^{26} \text{ cm}^{-2}$, exactly those we consider in our model.

An IceCube analysis was done for 14 objects [7]. Two objects from the original selection above were not analysed since they are located in the southern sky where IceCube has a lower sensitivity. On the other hand, NGC 3628 was added back in the IceCube analysis, since it was omitted from the original selection for its lack of X-ray emission above background, making it, however, an interesting target. The IceCube analysis finds no significant signal and gives an upper limit on the $E^2\Phi$ -flux for each of these objects, assuming an E^{-2} -flux between 1 TeV and 1 PeV. The final list of objects, their classification and the limits on their neutrino emission are shown in Table I.

Finally, it is important to remark that since almost all objects in this selection are a subset of blazars, it is unlikely that sources from this class (i.e. “obscured blazars”) are responsible for the bulk of the neutrino flux. However, this selection is interesting for two reasons. First, given the luminosity of these objects, they are good targets to test whether the model under consideration occurs in nature. Second, if the scenario is indeed applicable to these objects, the neutrino flux thus produced allows us to directly probe the amount of accelerated hadrons in these blazars.

B. Normalising the neutrino flux

In the following, we calculate the neutrino flux expected in our model for the objects in the final IceCube analysis cited above. We fix the column density to the benchmark values $N_H^{(1,2)}$, compatible with the values de-

rived for the objects individually, and investigate the resulting neutrino production.

Given the choice of benchmark values of N_H in our model, the only parameter left to determine in order to predict the neutrino flux from the set of objects selected above is the normalisation of the flux. The first selection criterion for the object selection presented in [29] was strong radio emission. Moreover, the radio flux is unattenuated by matter in between the source and the observer, giving a direct view of the inner engine, a feature which was also already exploited in this analysis. Therefore, it is natural to normalise the expected neutrino flux based on the radio flux.

The radio emission from astrophysical objects is typically attributed to synchrotron emission from accelerated electrons in the magnetic field of the source. Therefore, it is expected that the radio and electron luminosity are comparable in size. The exact relation between the radio and electron luminosities was derived in [33]. It is obtained by integrating the synchrotron emission from electrons of energy E_e , or equivalently γ_e , over the electron spectrum. Assume an electron spectrum $\frac{dN_e}{d\gamma_e} \propto \gamma_e^{-2}$, a minimum energy $\gamma_e^{\min} = \{1, 10\}$ (estimated from efficient cooling, i.e. strong radio emission of the electrons) and maximum energy $\gamma_e^{\max} = 10^9 - 10^{11}$ (corresponding to the assumption that protons are co-accelerated up to energies $10^{18} - 10^{21}$ eV). For these limits of the electron energy, the authors of [33] find that

$$\chi = \frac{L_e}{L_R} \approx 100, \quad (8)$$

over a large range of magnetic field strengths. Deviations from this value occur fastest for $\gamma_e^{\min} = 10$, with significant changes starting at 10 G. Modelling the properties of bright Fermi blazars, one finds that typical magnetic field strengths are between 0.1 – 2 G for BL Lacs and 1–10 G for FSRQs [90, 91]. Since the objects in our selection are assumed to be typical, apart from their obscuration, we use $\chi = 100$.

From the electron luminosity, we can obtain the proton luminosity, since these two species are co-accelerated. This has been discussed in detail by [82], from which we will repeat the main arguments here. Typically, one assumes that the number of accelerated protons and electrons are equal¹³, $N_e = N_p$ and that their spectral indices are the same. It is then straightforward to calculate the electron-proton luminosity ratio and this results in $f_e = \frac{L_e}{L_p} \approx 1/100$ [82, 92], which is true also for the differential luminosity (i.e. independent of energy). This result is supported by observations from the galaxy: when

¹³ From charge balance, this is true for the total number of electrons and protons. If the only requirement for initiating the acceleration is sufficient energy, this is then also true for the number of particles above the energy threshold, since in a plasma the particle energies follow a Maxwell-Boltzmann distribution which is independent of the particle mass [82].

TABLE I: Final objects in the obscured flat-spectrum radio AGN selection for which an IceCube analysis exists and the upper limit on their neutrino emission in units of 10^{-9} $\text{GeV cm}^{-2} \text{s}^{-1}$, from [7].

Name	RA ($^{\circ}$)	Dec ($^{\circ}$)	$E^2 \Phi_{\nu}^{90\%}$	Classification
PKS1717+177	259.80	17.75	0.754	BL Lac
CGCG186-048	176.84	35.02	0.856	BL Lac
RGBJ1534+372	233.70	37.27	0.899	BL Lac
NGC3628	170.07	13.59	0.719	Radio gal.
SBS1200+608	180.76	60.52	1.090	BL Lac
GB6J1542+6129	235.74	61.50	1.070	BL Lac
4C+04.77	331.07	4.67	0.650	BL Lac
MRK0668	211.75	28.45	0.879	FSRQ
3C371	271.71	69.82	1.180	BL Lac
B21811+31	273.40	31.74	0.850	BL Lac
SBS0812+578	124.09	57.65	1.090	BL Lac
2MASXJ05581173+5328180	89.55	53.47	1.080	FSRQ
1H1720+117	261.27	11.87	0.695	BL Lac
ARP220	233.74	23.50	0.746	ULIRG

comparing the observed electrons with cosmic rays up to the knee, one obtains a luminosity ratio 1/100. On the other hand, for extragalactic sources, this value is estimated to be closer to 1/10, obtained by comparing the observed radio luminosity with that of cosmic rays above the ankle. Since obtaining a more precise value requires extrapolating the extragalactic cosmic ray flux to energies below the ankle, with an unknown energy spectrum and minimum energy, this value is quite uncertain. Moreover, this extrapolation is dependent on the exact spectral index of extragalactic cosmic rays, which is still uncertain due to the degeneracy with composition and maximum energy. In case of a spectral index deviating from 2, the luminosity integral becomes very sensitive on the minimum energy, making a strong constraint on f_e difficult. However, for sure $f_e \ll 1$. From particle-in-cell simulations, it is found that the assumption of equal spectral indices for protons and electrons might not be true. In this case the luminosity ratio becomes energy dependent, further complicating the conversion from electron to proton luminosity. In the following, we will assume a fixed ratio

$$f_e = \frac{L_e}{L_p} = \frac{1}{10}, \quad (9)$$

which is conservative (i.e. relatively few protons).

Summarising, in order to determine the expected neutrino flux from the objects in the selection above, we integrate the observed radio flux from each object individually and convert this to a proton luminosity

$$L_p = \frac{\chi \cdot L_R}{f_e}. \quad (10)$$

A proton population with this total luminosity is then allowed to interact with a gas cloud of column density $N_H = N_H^{(1,2)}$. Note that it is not needed to convert the

observed flux to luminosity at the source, since the same factor d_L^2 appears when propagating the obtained neutrino flux at the source back to Earth.

C. Results

In this section, we present the neutrino flux predicted by our model for the objects in the obscured flat-spectrum AGN selection. For the simulation, we generate 5×10^4 events, with the proton energy between 100 GeV and 10^8 GeV and a spectral index of 2. The column density is set to either of the two benchmark values: $N_H^{(1)} = 5 \times 10^{25} \text{ cm}^{-2}$ or $N_H^{(2)} = 10^{26} \text{ cm}^{-2}$. As argued in Section IID, we include only gamma-ray attenuation at the source by matter, not radiation fields. While propagating to Earth, the gamma-ray flux is also attenuated by interaction with the EBL and CMB (this is discussed in more detail in Section VC). This attenuation, but not the full EM cascade to lower energy gamma rays, is included in the final gamma-ray flux¹⁴, using the optical depth $\tau(E_\gamma, z)$ for gamma rays at the redshift of the source from [93]

$$E_\gamma^2 \Phi_\gamma(E_\gamma) = e^{-\tau(E_\gamma, z)} E_\gamma^2 \Phi_\gamma^0(E_\gamma). \quad (11)$$

The hybrid spectral energy distribution (SED) for the object with the highest expected neutrino emission, 3C371, is shown in Figure 2, with $N_H^{(2)} = 10^{26} \text{ cm}^{-2}$.

¹⁴ This is the usual approach. For a point source, including the full cascade would require more detailed modelling than the simple approach of Section VC. Since the predicted gamma-ray flux turns out to be very low compared to the observed flux, the additional modelling is not important.

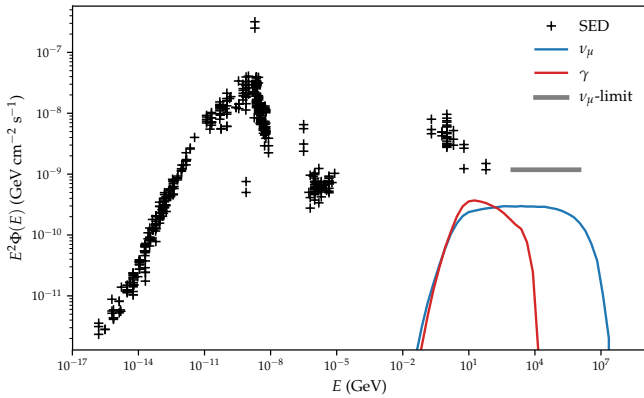


FIG. 2: Hybrid SED for 3C371, one of the objects with a predicted muon neutrino flux closest to the current upper limit [7], showing the measured electromagnetic data together with the predicted muon neutrino flux and gamma-ray flux in our obscured neutrino source model. Here we assumed $N_H^{(2)} = 10^{26} \text{ cm}^{-2}$ and $E_p \in [10^2, 10^8] \text{ GeV}$. Electromagnetic spectrum data from [95–121] retrieved using the `SSDC SED Builder` [122].

The figure includes the measured photon SED across all wavelengths, the predicted gamma-ray emission from pp -interactions, as well as the predicted muon neutrinos flux¹⁵ and the IceCube limit on the muon neutrino flux from this object. The SEDs of the other objects are shown in Appendix A. The predicted neutrino flux for 3C371 is well below the limit from IceCube, such that our model is not ruled out and could only be observable with next-generation cosmic neutrino detectors, such as IceCube Gen2 (with an estimated improvement of the point source sensitivity with a factor of about five over IceCube [94]). The gamma-ray flux from pp -interactions in this model is well below the observed flux from this object, leaving the model also unconstrained here.

The same conclusions are also true for the other objects in the selection. Their calculated neutrino fluxes can be found in Table II, for both $N_H^{(1)} = 5 \times 10^{25} \text{ cm}^{-2}$ and $N_H^{(2)} = 10^{26} \text{ cm}^{-2}$. The same results are shown in Figure 3, which also includes the flux in case the minimum proton energy is lowered to 1 GeV. For all objects, the predicted neutrino flux using natural choices for the values of the parameters χ and f_e is below the limit placed by IceCube. Given the expected sensitivity of IceCube Gen2, however, some of these objects could be observable in the near future in this model. The gamma-ray flux is in each case well below the observed value, putting no constraint on the model. This also immediately implies that, for this class of objects, there is

no constraint from the EGB, since their contribution is irrelevant compared to the blazar contribution already present. On the other hand, this also suggests that, even if this scenario were applicable to all blazars (which is certainly not true), the neutrino flux would not be high enough to explain the diffuse flux observed by IceCube.

The above results already allow us to put meaningful constraints on the only parameter which is not fixed by our model¹⁶: the electron-proton luminosity ratio, for which we took $f_e = 1/10$. Translating the IceCube limit to a lower bound on f_e (i.e. maximum amount of accelerated protons) in our model, we find a bound of $f_e \approx 0.001 - 0.02$. This is also shown in Table II and Figure 4. Since the galactic value of the electron-proton luminosity ratio is $f_e \approx 1/100$, these constraints on f_e within our model are already quite strong. The reason that these bounds are so strong, is that for the column densities considered here, the full proton population is depleted to produce neutrinos, as opposed to typical scenarios where only part of the proton flux interacts. The advantage of this was already discussed: even if such blazars are not the dominant source of astrophysical neutrinos, identifying a few obscured blazars gives independent constraints on the amount of accelerated protons in blazars.

Finally, we can also investigate an alternative calculation, where instead the predicted gamma-ray and neutrino flux are normalised to the observed gamma-ray flux as opposed to the radio flux. In the case of 3C371, this would lead to a neutrino emission comparable to the IceCube limit. However, in this case more detailed SED modelling is needed in order to explain the complete emission from this object. Moreover, not all objects in our selection have sufficient data to perform this analysis. Therefore, we refrain from doing this.

V. DIFFUSE FLUX FROM A GENERIC OBSCURED POPULATION

In this section, we calculate the diffuse neutrino and gamma-ray flux from a generic population of obscured sources. In particular, we investigate whether sources obscured by a gas with column density $N_H^{(1,2)}$ can be responsible for the astrophysical neutrino flux measured by IceCube, without violating the bound on the non-blazar contribution to the EGB.

For this calculation, we will not be limiting ourselves to sources similar to those in the selection of Section IV. Instead, we consider a generic population of obscured sources characterised only by their evolution with redshift, while their total energy budget will be fitted to reproduce the observed neutrino flux. From generic arguments [123], we know that a source class with a power

¹⁵ The muon neutrino flux is 1/3 of the total neutrino flux, assuming full mixing between the neutrino flavours. This is the reason why the neutrino flux is below the gamma ray flux.

¹⁶ Since we consider the value of χ to be quite robust.

TABLE II: Summary of the predicted muon neutrino flux compared to the upper limits on their muon neutrino flux (from [7]), for the objects in the obscured flat-spectrum radio AGN selection in units of 10^{-9} GeV cm $^{-2}$ s $^{-1}$, as well as the corresponding limits on f_e . Protons are injected within the energy range $E_p \in [10^2, 10^8]$ GeV and the considered column densities are $N_H^{(1)} = 5 \times 10^{25}$ cm $^{-2}$ and $N_H^{(2)} = 10^{26}$ cm $^{-2}$.

Name	$E^2 \Phi_\nu^{90\%}$	$E^2 \Phi_\nu^{(1)}$	$E^2 \Phi_\nu^{(2)}$	$f_e^{(1)}$	$f_e^{(2)}$
PKS1717+177	0.754	0.062	0.070	8.1×10^{-3}	9.2×10^{-3}
CGCG186-048	0.856	0.032	0.037	3.7×10^{-3}	4.2×10^{-3}
RGBJ1534+372	0.899	0.002	0.002	1.9×10^{-4}	2.2×10^{-4}
NGC3628	0.719	0.039	0.045	5.4×10^{-3}	6.1×10^{-3}
SBS1200+608	1.090	0.012	0.014	1.1×10^{-3}	1.2×10^{-3}
GB6J1542+6129	1.070	0.009	0.011	8.7×10^{-4}	9.9×10^{-4}
4C+04.77	0.650	0.069	0.079	1.0×10^{-2}	1.2×10^{-2}
MRK0668	0.879	0.155	0.176	1.7×10^{-2}	2.0×10^{-2}
3C371	1.180	0.240	0.274	2.0×10^{-2}	2.3×10^{-2}
B21811+31	0.850	0.015	0.017	1.7×10^{-3}	1.9×10^{-3}
SBS0812+578	1.090	0.008	0.009	7.0×10^{-4}	8.0×10^{-4}
2MASXJ05581173+5328180	1.080	0.028	0.032	2.6×10^{-3}	2.9×10^{-3}
1H1720+117	0.695	0.007	0.008	1.0×10^{-3}	1.1×10^{-3}
ARP220	0.746	0.031	0.035	4.0×10^{-3}	4.6×10^{-3}

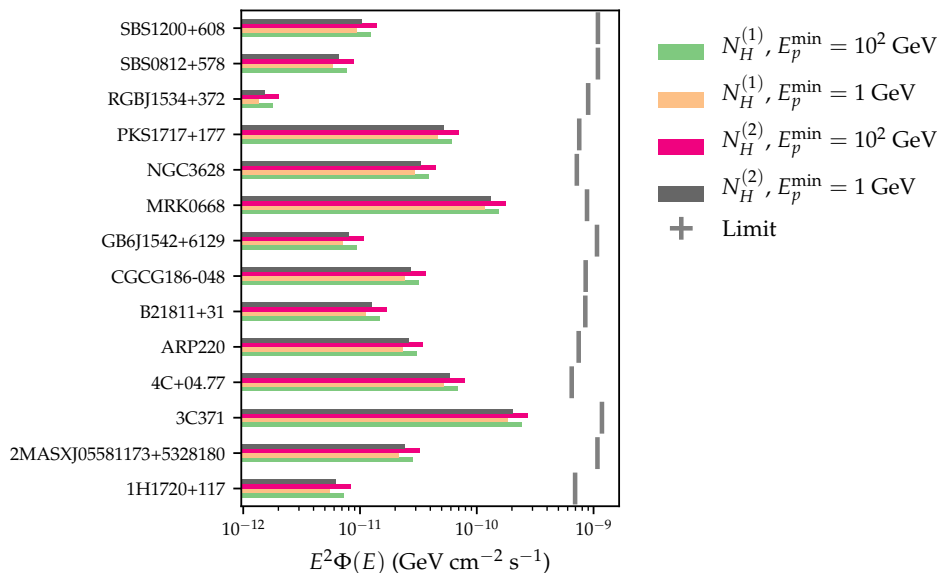


FIG. 3: Summary of the predicted muon neutrino flux in our obscured neutrino source model and the IceCube upper limits (from [7]) for the objects in the obscured flat-spectrum radio AGN selection.

similar to the UHECR sources can reproduce the flux observed by IceCube¹⁷. The only requirement on the source configuration is that throughout the history of the universe, a sufficiently large, possibly changing, population

of obscured sources exists. In our calculations, we do not assume the presence of a jet in such sources.

A. Populations

We consider the possibilities of redshift evolution following star formation, no evolution and the case of ULIRGs. One could also consider other scenarios, such as treating explicitly BL Lac and FSRQ evolution separately (see e.g. [14]).

¹⁷ Although, as we will see, we will end up requiring a maximum proton energy of $E_p \sim 10^8$ GeV in order to fit the IceCube flux and its upper limits at the higher energies. Therefore, these sources would not supply the UHECRs, but possess a similar energy budget.

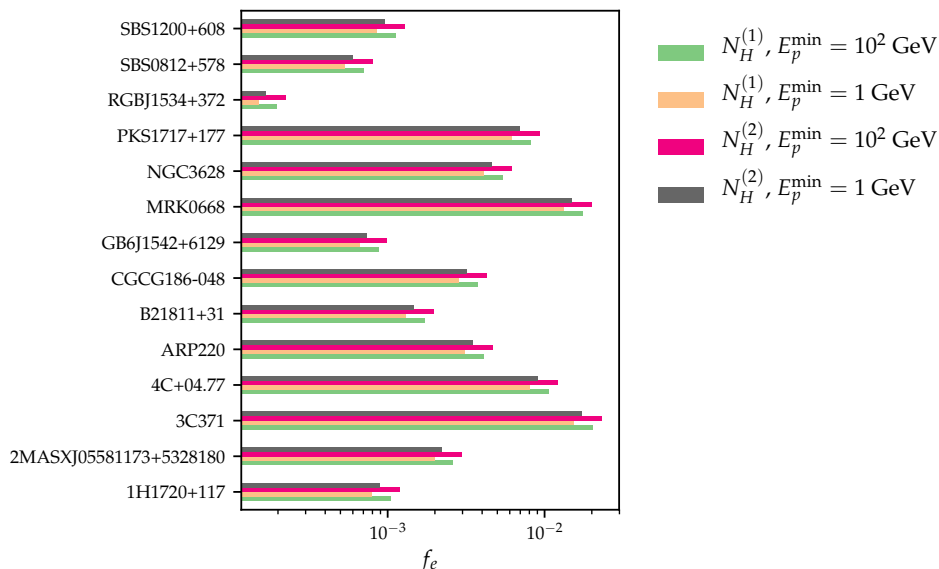


FIG. 4: Summary of the lower limits on f_e for the objects in the obscured flat-spectrum radio AGN selection.

1. Star formation rate and flat evolution

First, we consider a redshift evolution following the star formation rate. This is a natural choice, since it follows the evolution of galaxies throughout the cosmic history. This is particularly relevant for GRBs and supernovae, since these events occur more frequently during star formation when many large stars with short lifetimes are formed. It is also relevant for AGN- and blazar-like scenarios, since during intense star formation there could also be efficient accretion around supermassive black holes in the centres of galaxies. Even if the true rate deviates from the star formation rate, it is still a good first approximation for the amount of activity in galaxies as a function of redshift.

The star formation rate is measured using different observables, such as the supernova rate, luminosity densities, limits on the diffuse neutrino background from supernovae and GRBs. The star formation rate is well-known up to redshifts of $z \approx 1$. At higher redshifts, measurements deviate, although the knowledge is improving. In the following, we will use the star formation history derived in [124, 125]. Its form is

$$\mathcal{H}_{\text{SFR}} \propto (1+z)^{n_i}, \quad (12)$$

with

$$n_i = \begin{cases} 3.4 & z < 1 \\ -0.3 & 1 < z < 4 \\ -3.5 & z > 4. \end{cases} \quad (13)$$

The normalisation is such that $\mathcal{H}_{\text{SFR}}(z=0) = 1$ and the function is continuous.

As an alternative to cosmic star formation, we consider

also the simplest case of no evolution

$$\mathcal{H}_{\text{flat}} = 1. \quad (14)$$

2. Ultra-luminous infrared galaxies

In addition to the above generic scenarios, we will also consider in more detail the possibility that ultra-luminous infrared galaxies (ULIRG) could be responsible for the astrophysical neutrino flux detected by IceCube through our model. ULIRGs showed up already in the object selection used in Section IV A, where ARP 220 was a candidate object in the final selection. ARP 220 is the most well-known and best studied ULIRG and is an object with a very high IR luminosity formed by the merger of two galaxies, with a very high column density of at least 10^{25} cm^{-2} due to gas and dust. Its nucleus is possibly powered by an AGN, which must however be obscured and Compton-thick. [126].

More generally, ULIRGs are defined as galaxies with extreme infrared luminosities $L_{\text{IR}} > 10^{12} L_{\odot}$ (see e.g. the review [127]). They are the mergers of gas rich galaxies, with the central regions harbouring huge amounts of gas and dust. The emission is caused by starburst activity (i.e. high star formation rate), and possibly also AGN activity, triggered by the merger [128]. It is believed that submillimetre galaxies are the high-redshift counterparts of local ULIRGs.

The abundance and importance of AGN activity compared to starburst activity in ULIRGs is still not completely clear. Surveys indicate that ULIRGs contain radio cores which are due to AGN activity [129]. In studies of local ULIRGs [130], it was found that all of them require starburst activity to explain their emission, while

only half require an AGN. Moreover, in 90% of the cases, the starburst activity provides over half of the IR luminosity, with an average fractional luminosity of 82%. The AGN contribution does not increase with luminosity. Other studies have found that over half of the ULIRGs contain an AGN, with the fraction increasing with total IR luminosity [131]. In [132], it was found that only few ULIRGs are dominated by AGNs (5% at $z \sim 1$ and 12% at $z \sim 2$) although, at a given luminosity, the fraction of AGN activity is lower in high- z ULIRGs. In a $5 - 8 \mu\text{m}$ analysis [133] of local ULIRGs, signatures of AGN activity were found in $\sim 70\%$ of the sample. While most of the luminosity is due to the starburst activity, $\sim 23\%$ is due to the AGN, increasing with luminosity. More general, part of the emission of star-forming galaxies at high redshifts can be explained by AGN activity [134]. So, while AGNs are in general definitely not the dominant component of ULIRGs emission, their contribution is not negligible. Moreover, high obscuration of the central core may lead to underestimation of the AGN power [127].

The exact interplay between the central AGN and the starburst activity is still unclear. Several scenarios are still possible: one could evolve from the other, trigger the other or their coexistence might be coincidental. Typically, the AGN and ULIRG activity is unified in an evolutionary scenario. Early on in the merger, starburst activity is high when there is still plenty of gas. This merger might also relate to the growth of a supermassive black hole and AGN activity at the core [135]. This was confirmed by observations of stellar kinematics [136, 137]. Later, when the gas is concentrated in a compact region in the centre, a starburst-ULIRG phase occurs. During the late merger state, there is a high accretion rate at the centre, giving rise to an obscured QSO¹⁸/AGN-powered ULIRGs, due to the huge amount of gas and dust driven to the centre. Afterwards, the galaxy enters its most luminous phase with an optically-visible QSO which drives out the remaining material [127, 138]. In this sense, neutrino emission from ULIRGs would have an interesting interplay with galaxy formation and evolution.

Estimates of the space densities of ULIRGs have been made by several groups. In [139], they found at $z = 0.15$ that $n = 3 \times 10^{-7} \text{ Mpc}^{-3}$ for $L_{\text{IR}} = 1.6 \times 10^{12} L_{\odot}$ and $n = 9 \times 10^{-8} \text{ Mpc}^{-3}$ for $L_{\text{IR}} = 2.5 \times 10^{12} L_{\odot}$. This decreases with a factor 1.5 to lower redshift ($z = 0.04$), while it increase to $\Phi(L > 10^{11} L_{\odot}) = 1 - 3 \times 10^{-2} \text{ Mpc}^{-3}$ at $z \sim 1-3$. A full luminosity function was derived in [140], although their analysis is only sensitive to $L_{\text{IR}} > 10^{12.3} L_{\odot}$. In the same redshift range $z \sim 1-3$, they find $n > 6 \times 10^{-6} \text{ Mpc}^{-3}$. This leads to a redshift evolution

$$\mathcal{H}_{\text{ULIRG}} \propto \begin{cases} (1+z)^4 & z \leq 1 \\ \text{const.} & 1 < z < 4, \end{cases} \quad (15)$$

which we will use in the following, although other studies

found more extreme evolution up to $\propto (1+z)^7$ for $z = 0 - 1.5$ [141].

We will consider the central AGN, obscured by gas and dust driven to the centre by the merger, as a potential target for the obscured pp -neutrino production mechanism. ULIRGs have been considered before as the source of astrophysical neutrinos [27, 142], but in the context of cosmic-ray reservoir models, through confined cosmic rays interacting with gas in the galaxy. Instead, we consider only neutrino production in a compact region near the core. This region can have a very high column density, despite the overall surface gas density of starburst being only about 1 g cm^{-2} , or $N_H \sim 10^{23} \text{ cm}^{-2}$, much lower than the densities required by our mechanism. However, this overall surface gas density is only valid for the overall gas density, which is derived using the Kennicutt-Schmidt law [143–145] relating the star-formation rate with the gas density, and does not exclude the existence of local, compact objects or regions with higher densities. Finally, in our accelerator model, the cut-off of the proton and neutrino spectra can be at higher energy than in reservoir models, since there is no confinement criterion, although we will keep the cut-off at 10^8 GeV in order to not overshoot the IceCube flux at high energies.

Now, we can estimate whether ULIRGs can provide the required luminosity to supply the diffuse neutrino flux. Using the more conservative value $n \approx 5 \times 10^{-7} \text{ Mpc}^{-3}$ (integrating over luminosity) of the number densities quoted above, along with the minimum ULIRG luminosity $L_{\text{IR}} = 10^{12} L_{\odot}$, we estimate their local energy generation rate in the IR

$$\mathcal{Q}_{\text{IR}} = n(z=0) \cdot L_{\text{IR}}, \quad (16)$$

Afterwards, this IR luminosity is converted to radio luminosity using the radio-IR relation for ULIRGs [146]. Using the thermal infrared luminosity $L_{\text{TIR}} \equiv L(8 - 1000 \mu\text{m})$, the TIR/radio flux ratio is defined as

$$q_{\text{TIR}} = \log \left(\frac{L_{\text{TIR}}}{3.75 \times 10^{12} \text{ W}} \right) - \log \left(\frac{L_{1.4 \text{ GHz}}}{\text{W Hz}^{-1}} \right). \quad (17)$$

On average, this ratio has the value $\langle q_{\text{TIR}} \rangle = 2.6$, with no evolution in redshift. After obtaining $L_{1.4 \text{ GHz}}$ from this relation, we estimate the total radio luminosity as $L_R = 1.4 \text{ GHz} \times L_{1.4 \text{ GHz}}$. Using the relations in Section IV B, the radio luminosity can be converted into the proton luminosity (or energy generation rate) $\mathcal{Q}_p = \frac{\chi \cdot \mathcal{Q}_R}{f_e}$. We find

$$\mathcal{Q}_p^{\text{ULIRG}} \approx 10^{43.4} \text{ erg Mpc}^{-3} \text{ yr}^{-1}. \quad (18)$$

This luminosity is slightly below the value estimated in the Waxman-Bahcall calculation [123], such that ULIRGs do not initially seem capable of explaining the full astrophysical neutrino flux. Moreover, in this calculation it was assumed that all of the ULIRG luminosity is related to AGN activity, while in reality the AGN

¹⁸ Quasi-stellar object or quasar

contribution to the luminosity is at least one order of magnitude lower (integrated over all ULIRGs). On the other hand, we assumed that all ULIRGs have exactly $L_{\text{IR}} = 10^{12} L_{\odot}$, while many have higher luminosity. In addition, we used the standard value for the parameter f_e , while it can easily be lower by at least an order of magnitude, increasing \mathcal{Q}_p by the same factor.

B. Diffuse neutrino flux

In order to obtain the total diffuse flux of neutrinos from all sources in the observable universe, we need to perform an integral over cosmic history or, equivalently, over cosmological distance. Following the method in [12, 147, 148], the diffuse flux is given by

$$E_{\nu}^2 \Phi_{\nu}^{\text{diffuse}}(E_{\nu}) = \frac{c}{4\pi H_0} \int \frac{\mathcal{H}(z)}{(1+z)^2 E(z)} \times \varepsilon_{\nu} \mathcal{Q}_{\varepsilon_{\nu}}(\varepsilon_{\nu})|_{\varepsilon_{\nu}=(1+z)E_{\nu}} dz, \quad (19)$$

under the assumption that the redshift evolution can be factorised out of the luminosity function. The factor $\mathcal{Q}_{E_{\nu}}(E_{\nu})$ is defined as $\mathcal{Q}_{E_{\nu}}(E_{\nu}) = E_{\nu} \Phi_{\nu}(E_{\nu})$, such that $\int dE_{\nu} E_{\nu} \Phi_{\nu}(E_{\nu}) = \mathcal{Q}_{\nu}$, with \mathcal{Q}_{ν} the total injected neutrino luminosity per comoving volume. Its form is obtained from our numerical simulation, where the normalisation of $\mathcal{Q}_{E_{\nu}}$ is free to be determined either by fitting the final diffuse flux $\Phi_{\nu}^{\text{diffuse}}$ or by fixing the total injected proton luminosity.

The z -integral becomes energy-independent for the case of a power law spectrum¹⁹ $\mathcal{Q}_{E_{\nu}} \propto E_{\nu} \cdot E_{\nu}^{-\gamma}$ and the previous assumption that the redshift evolution and $\mathcal{Q}_{E_{\nu}}(E_{\nu})$ are independent. We then get

$$\xi_z = \int \frac{dz}{E(z)} \mathcal{H}(z) (1+z)^{-\gamma}, \quad (20)$$

which can be solved numerically. The simplified formula for the final flux then becomes the standard result [123]

$$E_{\nu}^2 \Phi_{\nu}^{\text{diffuse}}(E_{\nu}) = \frac{c}{4\pi} \xi_z \frac{1}{H_0} E_{\nu} \mathcal{Q}_{E_{\nu}}(E_{\nu}). \quad (21)$$

For the case of $\gamma = 2$, we find $\xi_z = 2.4$ for a redshift evolution following star formation $\mathcal{H}(z) = \mathcal{H}_{\text{SFR}}(z)$ (Eqs. (12) and (13)). For no evolution we have $\xi_z = 0.53$ and for the case of ULIRGs, we find $\xi_z = 3.6$.

¹⁹ I.e. this is no longer true once we include a cut-off (e.g. an exponential) in the spectrum. This agrees with the intuition that the contribution from the end of the spectrum changes with redshift. However, as long as we calculate the flux at an energy sufficiently far from the cut-off, the calculation for a power law is valid. For our own result, we use the full integral, which does not suffer from this subtlety.

C. Diffuse gamma-ray flux

In order to obtain the diffuse gamma-ray background from the neutrino sources considered here, an additional effect needs to be taken into account. During propagation, gamma rays can interact with the extragalactic background light (EBL) and the cosmic microwave background (CMB), producing an e^+e^- -pair. The gamma-ray flux from redshift z is thus cut off above the energy where the optical depth in the EBL becomes equal to 1. In turn, these electrons can up-scatter EBL and CMB photons back to gamma-ray energies through inverse-Compton scattering or by emitting synchrotron radiation, initiating an electromagnetic cascade. In this way photons of energies above ~ 100 GeV are reprocessed and accumulate at energies at and below 100 GeV, significantly increasing the flux at these energies.

We follow the procedure outlined in [11] in order to calculate the gamma ray spectrum after cascading in the EBL analytically. As described in [149, 150], after the EM cascade has sufficiently developed, it attains a universal form given by (using $G_{E_{\gamma}} = E_{\gamma} \Phi_{\gamma}$ in order to denote the cascade)

$$G_{E_{\gamma}} \propto \begin{cases} \left(\frac{E_{\gamma}}{E_{\gamma}^{\text{br}}}\right)^{-1/2} & (E_{\gamma} < E_{\gamma}^{\text{br}}) \\ \left(\frac{E_{\gamma}}{E_{\gamma}^{\text{br}}}\right)^{1-\beta} & (E_{\gamma}^{\text{br}} < E_{\gamma} < E_{\gamma}^{\text{cut}}), \end{cases} \quad (22)$$

normalised to $\int dE_{\gamma} G_{E_{\gamma}} = 1$. Typically, $\beta \approx 2$. The cut-off energy E_{γ}^{cut} is the energy where suppression due to pair production occurs. It can be obtained from the requirement²⁰ $\tau(E_{\gamma}^{\text{cut}}, z) = 1$, for which we use the optical depth tables provided in [93]. The break energy is given by²¹ $E_{\gamma}^{\text{br}} \approx \frac{4}{3} \left(\frac{E_{\gamma}^{\text{cut}}}{2m_e c^2}\right)^2 \varepsilon_{\text{CMB}} \approx 0.034 \text{ GeV} \left(\frac{E_{\gamma}^{\text{cut}}}{0.1 \text{ TeV}}\right)^2 \left(\frac{1+z}{2}\right)^2$, where ε_{CMB} is the typical CMB energy. Above the cut-off energy E_{γ}^{cut} , but below $\min\left[\frac{E_{\gamma}^{\text{max}}}{2}, \frac{4}{3} \left(\frac{E_{\gamma}^{\text{max}}}{2m_e c^2}\right)^2 \varepsilon_{\text{CMB}}\right]$, the cascade is not sufficiently developed and its exact form depends on the details of the injection. With far away sources, for gamma rays scattering in the Thompson regime one can assume a simple exponential cut-off $e^{-\tau_{\gamma\gamma}}$ for $d > \lambda_{\gamma\gamma}$ with $\tau_{\gamma\gamma}(E_{\gamma}, z) = d(z)/\lambda_{\gamma\gamma}(E_{\gamma})$. On the other hand, in

²⁰ As opposed to the formula in [150], where an extra factor $(1+z)$ is included in the energy.

²¹ This break energy is due to the lowest energy at which electrons are created that can up-scatter photons from the CMB through inverse-Compton scattering. From the energy loss rate of an electron through IC scattering and the number of photons scattered per unit time, one finds the average energy of scattered photons as $\varepsilon_{\gamma} \approx \frac{4}{3} \gamma_e^2 \varepsilon_{\text{CMB}}$, with γ_e the Lorentz factor of the electron. This roughly corresponds to the handwaving argument that the photons gains two Lorentz factors of energy: one from transforming to the electron frame (where scattering is easy) and one from transforming back.

the Klein-Nishina regime pairs are continuously supplied, giving a shape $\frac{1-e^{-\tau_{\gamma\gamma}}}{\tau_{\gamma\gamma}}$ as long as the pair injection length (λ_{BH}) is longer than d . For our purposes, we use the exponential form, although the exact details do not significantly influence our conclusion. For more details with a full numerical calculation of the cascade, see [151–153].

Finally, the full diffuse spectrum is obtained by integrating the cascaded spectrum from each redshift and weighting with the injected luminosity from each redshift, giving

$$E_\gamma^2 \Phi_\gamma(E_\gamma) = \frac{c}{4\pi} \frac{1}{H_0} \int \frac{\mathcal{H}(z) dz}{(1+z)^2 E(z)} E_\gamma G_{E_\gamma} \mathcal{Q}_\gamma. \quad (23)$$

The factor \mathcal{Q}_γ is the total integrated luminosity in gamma rays per comoving volume injected by the sources (after attenuation by the gas column) and is obtained from our simulation.

From the integrand, we see that the dominant injection is from sources at $z \sim 1$, so that we can estimate the diffuse gamma-ray flux as [11]

$$E_\gamma^2 \Phi_\gamma(E_\gamma) \approx \frac{c}{4\pi} \frac{1}{H_0} \xi_z E_\gamma G_{E_\gamma} \Big|_{z=1} \mathcal{Q}_\gamma, \quad (24)$$

with $E_\gamma G_{E_\gamma} \Big|_{z=1} \approx 0.1$ between the break and the cut-off. Since the cut-off energy at $z = 1$ is about 100 GeV, there will be an accumulation²² of gamma rays at this energy, which is then also typically the point most strongly constrained by the Fermi measurements.

In order to get the full spectrum, however, this simple approximation is not sufficient and we need to do the full integration of Eq. (23) numerically. As a consequence of this complicated integration over redshift, the gamma-flux is sensitive to the details of the redshift evolution, in contrast to the neutrino flux where there is a degeneracy between the evolution (through ξ_z) and the normalisation.

We also verified the resulting spectrum ourselves with a numerical simulation using `CRPropa 3` [154] and its `DINT` module, which follows the description in [155]. We find that the resulting spectrum has the same form.

D. Results

The diffuse flux for the different redshift evolutions above and the assumed column densities $N_H^{(1)} = 5 \times 10^{25} \text{ cm}^{-2}$ and $N_H^{(2)} = 10^{26} \text{ cm}^{-2}$ are calculated using our Monte Carlo simulation, generating 5×10^4 events

with proton energy between 100 GeV and 10^8 GeV. The injected proton energy budget is then normalised by fitting the resulting neutrino spectrum (taking into account a flavour factor 1/3 after oscillation) to the single-flavour neutrino flux observed by IceCube [4]. The results of this calculation are shown in Figure 5, where the gamma ray flux can be compared to the bound on the non-blazar contribution to the EGB (both the best fit (14%) and its weakest upper limit (28%) [18–24]). These results can be compared with Figure 6, which shows the result for the same situation in case there is no attenuation of the gamma rays. This comparison seems a bit artificial (although it serves only to show the effect of obscuration in our model), since these large column densities automatically imply that attenuation is present. Physically, it might be more relevant to compare with the case $N_H = 10^{24} \text{ cm}^{-2}$ if one is interested in the effect of the higher density. This change lowers both the attenuation of gamma rays and the fraction of protons that interact²³, the latter of which needs to be compensated for by increasing the injected proton luminosity to fit the IceCube flux. In the end, only the neutrino luminosity normalisation and its correlation with the gamma ray luminosity are then important. On the other hand, in cosmic ray reservoir models, the protons effectively cross a high density target, while the gamma rays escape immediately. This then corresponds to the high density case shown here with gamma-ray attenuation turned off.

We find that in the case of a redshift evolution following star formation \mathcal{H}_{SFR} or the ULIRG evolution $\mathcal{H}_{\text{ULIRG}}$, the bounds from the non-blazar contribution to the EGB can be satisfied, as opposed to the case in which there is no attenuation, although in the case $N_H^{(1)} = 5 \times 10^{25} \text{ cm}^{-2}$ the improvement is small. In the case of a flat evolution $\mathcal{H}_{\text{Flat}}$, in which the contribution from low- z sources is more important, this bound can not be satisfied for $N_H^{(1)} = 5 \times 10^{25} \text{ cm}^{-2}$ and only marginally for $N_H^{(2)} = 10^{26} \text{ cm}^{-2}$.

The fitted proton energy budgets for all the cases are shown in Table III. For the case of ULIRGs, these can be compared with the optimistic estimate from Section V A 2. We find that even this estimate, which did not take into account that most of the ULIRG luminosity is due to starburst activity instead of a central engine, is about one order of magnitude too low. In order to explain the diffuse neutrino flux with objects like ULIRGs, other object classes are therefore necessary. The slightly less luminous LIRG²⁴ are candidates for this. On the other hand, the estimate also depended on the electron-proton luminosity ratio f_e . Lowering this ratio can already in-

²² This accumulation does indeed rise above the hypothetical flux in the absence of attenuation, since the non-attenuated spectrum can be substituted in Eq. (24) by replacing the factor $E_\gamma G_{E_\gamma}$ by $1/\ln\left(\frac{E_\gamma^{\text{max}}}{E_\gamma^{\text{min}}}\right)$. With an injected energy range between $E_p^{\text{max}}/20$ and $\ll 1$ GeV from pion decays, this is smaller than 0.1.

²³ It also is more sensitive to the energy dependence of the proton-proton cross section, such that the neutrino spectrum is flatter than that of the original protons.

²⁴ Galaxies with luminosities $L > 10^{11} L_\odot$, which are more numerous than e.g. starburst galaxies.

TABLE III: Required proton luminosities \mathcal{Q}_p from the fit to the observed IceCube single-flavour neutrino flux, in units of 10^{45} erg Mpc $^{-3}$ yr $^{-1}$.

Evolution	\mathcal{H}_{SFR}	$\mathcal{H}_{\text{Flat}}$	$\mathcal{H}_{\text{ULIRG}}$
Column density			
$N_H^{(1)} = 5 \times 10^{25} \text{ cm}^{-2}$	2.30	9.71	1.60
$N_H^{(2)} = 10^{26} \text{ cm}^{-2}$	2.17	9.18	1.51

crease the contribution from ULIRGs significantly.

Finally, we show in Figure 7 results of the same calculation for a proton index $\gamma = 2.1$. In this case, only the highest density $N_H^{(2)} = 10^{26} \text{ cm}^{-2}$ can marginally satisfy the constraints from the non-blazar contribution to the EGB for \mathcal{H}_{SFR} and $\mathcal{H}_{\text{ULIRG}}$.

VI. CONCLUSION

In this work, we investigated the possibility that AGN obscured by matter emit high energy neutrinos created in pp -interactions with a gas of a sufficiently high column density which acts as a beam dump. In this case, neutrino production can be efficient, whilst the produced gamma rays can at the same time be attenuated through pair production by the same gas cloud. Here, we took as benchmark values for the column density $N_H^{(1)} = 5 \times 10^{25} \text{ cm}^{-2}$ and $N_H^{(2)} = 10^{26} \text{ cm}^{-2}$.

First, we calculated the neutrino spectra emitted from a set of active galaxies whose electromagnetic spectrum can be explained with obscuration by matter. The selection, performed in [29], searches for strong radio-emitting galaxies with a lower-than-expected X-ray flux. The resulting objects are mainly blazars, along with one radio galaxy and one ULIRG. The candidate class of obscured blazars, being a subset of blazars, is unlikely to be responsible for the bulk of the IceCube flux, since their number density is too low. Still, they are interesting targets to test the viability of our model. Moreover, neutrino emission from such objects would provide a simple measurement of the accelerated proton content of blazars. We found that the predicted neutrino emission from these objects is below the limit set by IceCube, leaving the model unconstrained. For several of these objects, the scenario can be tested in the future upgrade of IceCube, IceCube-Gen2, while for many of them the predicted neutrino flux is too low to be detected in the near future. On the other hand, current limits already allow to constrain the amount of accelerated protons in blazars, with values $f_e > 0.001$ – 0.02 .

Second, we investigated the diffuse neutrino and gamma-ray flux from an unspecified population of neutrino sources operating under our model. In particular, we tested whether obscured pp -neutrino sources can be the source of the IceCube flux without violating the bounds on the non-blazar contribution to the EGB. In

the case of a redshift evolution following star formation or for ULIRGs, this is indeed possible for both $N_H^{(1)} = 5 \times 10^{25} \text{ cm}^{-2}$ and $N_H^{(2)} = 10^{26} \text{ cm}^{-2}$, although in the former case the gamma-ray flux is close to the EGB bound. In the case of no evolution with redshift, the EGB bound is violated. This conclusion is valid for a neutrino spectrum $\propto E_\nu^{-2}$, which has trouble explaining the low energy events recorded by IceCube (although this can be solved with a second distinct population). In the case of steeper spectra, the constraints are more tight. Even for the thickest gas clouds considered here, the gamma-ray flux is just barely below the EGB limit.

We also discussed in more detail whether a specific source class of special interest for our model, ULIRGs, could be responsible for the IceCube flux. Since ULIRGs occur when two galaxies merge, neutrino emission from such objects could have an interesting interplay with galaxy formation and evolution. While the predicted neutrino and gamma-ray flux are compatible with observation²⁵, a simple, optimistic, estimate of their the proton luminosity \mathcal{Q}_p of the complete population undershoots the required value. However, this conclusion depends on the electron-proton luminosity ratio f_e , for which we assumed a conservative value 1/10. Taking lower values boosts the amount of accelerated protons, increasing the provided luminosity. Another possibility is that also the slightly less luminous LIRG contribute through the same scenario. In this sense, a separate analysis of the highly obscured LIRG NGC 4418 would be interesting.

Finally, the same scenario could also be applicable to other objects. One intriguing, though speculative, possibility is that AGNs in the early universe can produce neutrinos through our model when they first turn on. At this time, a lot of gas and dust is still surrounding the centres of galaxies, potentially providing an ideal target. While these early AGNs might not explain the full IceCube neutrino flux (even more so because then the connection with the observed total gamma-ray energy budget is less obvious), they could make up part of it. This high- z flux would constitute an unresolvable component of the total neutrino flux. Moreover, gamma-rays from such a high redshift would be cascaded down to lower energy than from $z = 1$ -sources, such that the Fermi bounds from such a population are much less stringent. Moreover, like ULIRGs, such a scenario would tie neutrino production to galaxy formation and evolution.

²⁵ The gamma-ray flux might even be more attenuated by interactions at high energy with the IR field present in these galaxies, see e.g. [28].

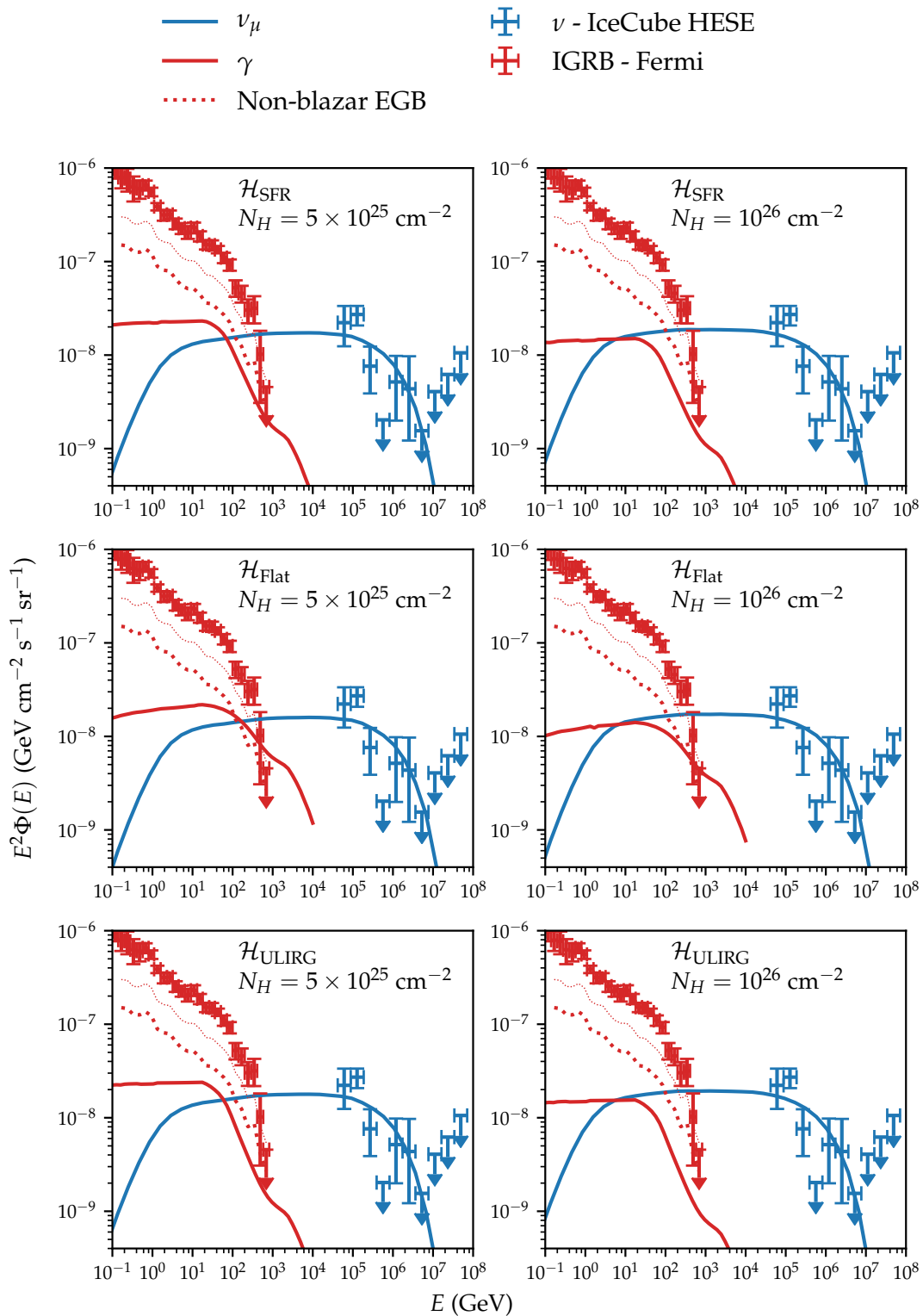


FIG. 5: Results for the diffuse neutrino and gamma-ray flux, for different evolutions and column densities for the obscured pp -neutrino scenario, fitted to the IceCube single-flavour neutrino flux (HESE) [4], for a spectral index of 2 and proton energy between 100 GeV and 10^8 GeV. The non-blazar contribution to the EGB shows both the best fit value (14% of the EGB measured by Fermi [156]) and the weakest upper limit (28%).

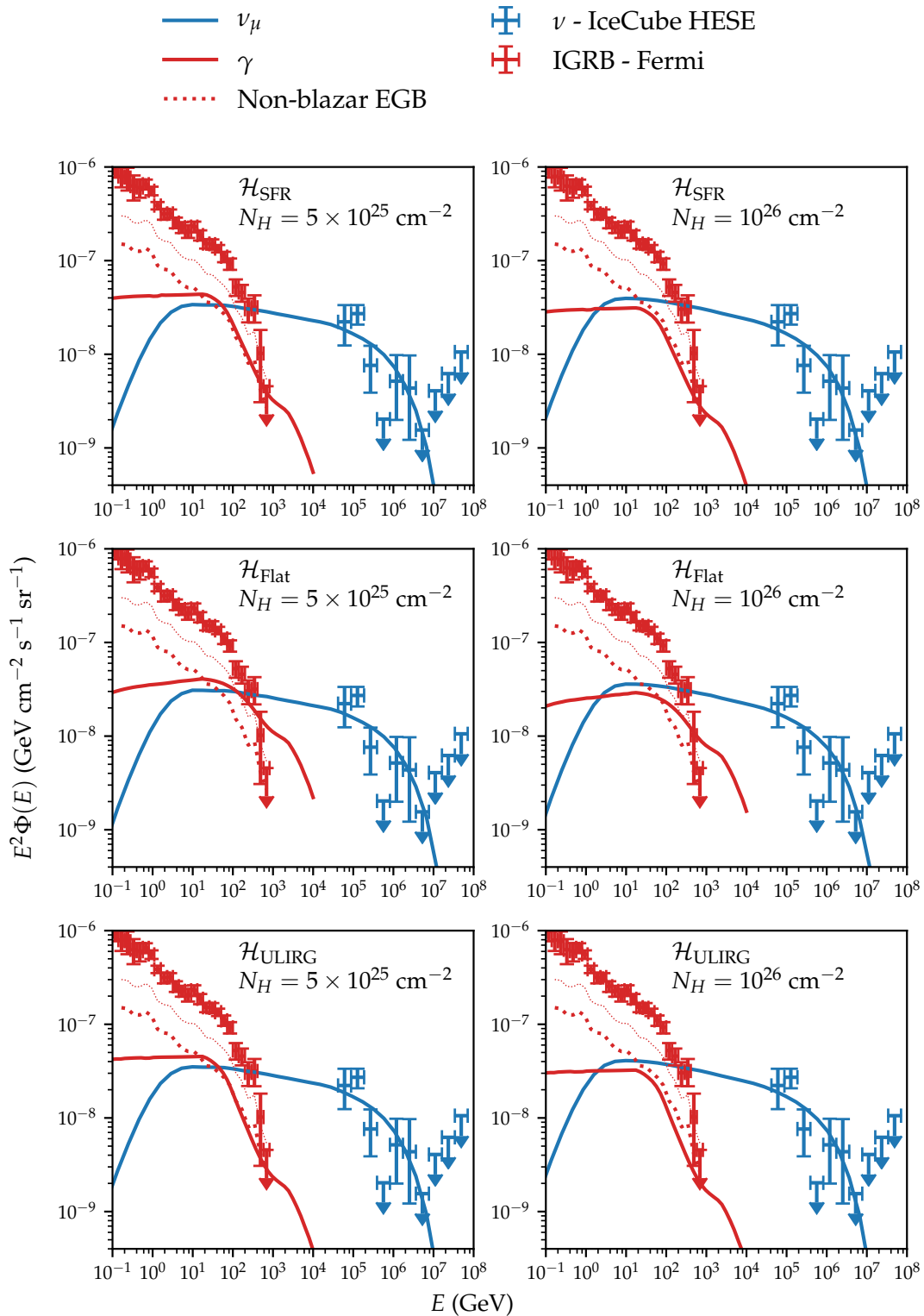


FIG. 7: Same as Figure 5, now with proton spectral index $\gamma = 2.1$.

Acknowledgments

This work was performed while MV was aspirant FWO Vlaanderen. KdV was supported in by the Flemish Foundation for Scientific Research FWO-12L3715N, and the European Research Council under the EU-ropean Unions Horizon 2020 research and innovation programme (grant agreement No 805486).

Appendix A: SED of all the objects

Figures 8, 9 and 10 show the hybrid SED for all other objects in the obscured flat-spectrum radio AGN se-

lection, as shown for 3C371 in Figure 2, for $N_H^{(2)} = 10^{26} \text{ cm}^{-2}$.

Appendix B: Object citations

In table IV we list the publications used for the datapoints used in Figures 2, 8, 9, and 10, retrieved using SED Builder [122].

-
- [1] Kohta Murase, Foteini Oikonomou, and Maria Petropoulou. Blazar Flares as an Origin of High-Energy Cosmic Neutrinos? *Astrophys. J.*, 865(2):124, 2018. doi: 10.3847/1538-4357/aada00.
 - [2] Dan Hooper, Tim Linden, and Abby Vieregge. Active Galactic Nuclei and the Origin of IceCube’s Diffuse Neutrino Flux. *JCAP*, 1902:012, 2019. doi: 10.1088/1475-7516/2019/02/012.
 - [3] Andrea Palladino, Xavier Rodrigues, Shan Gao, and Walter Winter. Interpretation of the diffuse astrophysical neutrino flux in terms of the blazar sequence. *Astrophys. J.*, 871(1):41, 2019. doi: 10.3847/1538-4357/aaf507.
 - [4] M. G. Aartsen et al. The IceCube Neutrino Observatory - Contributions to ICRC 2017 Part II: Properties of the Atmospheric and Astrophysical Neutrino Flux. 2017.
 - [5] M. G. Aartsen et al. Search for steady point-like sources in the astrophysical muon neutrino flux with 8 years of IceCube data. *Eur. Phys. J.*, C79(3):234, 2019. doi: 10.1140/epjc/s10052-019-6680-0.
 - [6] M. G. Aartsen et al. The contribution of Fermi-2LAC blazars to the diffuse TeV-PeV neutrino flux. *Astrophys. J.*, 835(1):45, 2017. doi: 10.3847/1538-4357/835/1/45.
 - [7] M. G. Aartsen et al. The IceCube Neutrino Observatory - Contributions to ICRC 2017 Part I: Searches for the Sources of Astrophysical Neutrinos. 2017.
 - [8] M. G. Aartsen et al. Extending the search for muon neutrinos coincident with gamma-ray bursts in IceCube data. *Astrophys. J.*, 843(2):112, 2017. doi: 10.3847/1538-4357/aa7569.
 - [9] Paolo Lipari. Proton and Neutrino Extragalactic Astronomy. *Phys. Rev.*, D78:083011, 2008. doi: 10.1103/PhysRevD.78.083011.
 - [10] A. Silvestri and S. W. Barwick. Constraints on extragalactic point source flux from diffuse neutrino limits. *Phys. Rev. D*, 81(2):023001, January 2010. doi: 10.1103/PhysRevD.81.023001.
 - [11] Kohta Murase, John F. Beacom, and Hajime Takami. Gamma-Ray and Neutrino Backgrounds as Probes of the High-Energy Universe: Hints of Cascades, General Constraints, and Implications for TeV Searches. *JCAP*, 1208:030, 2012. doi: 10.1088/1475-7516/2012/08/030.
 - [12] Markus Ahlers and Francis Halzen. Pinpointing Extragalactic Neutrino Sources in Light of Recent IceCube Observations. *Phys. Rev.*, D90(4):043005, 2014. doi: 10.1103/PhysRevD.90.043005.
 - [13] Marek Kowalski. Status of High-Energy Neutrino Astronomy. *J. Phys. Conf. Ser.*, 632(1):012039, 2015. doi: 10.1088/1742-6596/632/1/012039.
 - [14] Kohta Murase and Eli Waxman. Constraining High-Energy Cosmic Neutrino Sources: Implications and Prospects. *Phys. Rev.*, D94(10):103006, 2016. doi: 10.1103/PhysRevD.94.103006.
 - [15] Kohta Murase, Markus Ahlers, and Brian C. Lacki. Testing the Hadronuclear Origin of PeV Neutrinos Observed with IceCube. *Phys. Rev.*, D88(12):121301, 2013. doi: 10.1103/PhysRevD.88.121301.
 - [16] Irene Tamborra, Shin’ichiro Ando, and Kohta Murase. Star-forming galaxies as the origin of diffuse high-energy backgrounds: Gamma-ray and neutrino connections, and implications for starburst history. *JCAP*, 1409:043, 2014. doi: 10.1088/1475-7516/2014/09/043.
 - [17] Keith Bechtol, Markus Ahlers, Mattia Di Mauro, Marco Ajello, and Justin Vandenbroucke. Evidence against star-forming galaxies as the dominant source of IceCube neutrinos. *Astrophys. J.*, 836(1):47, 2017. doi: 10.3847/1538-4357/836/1/47.
 - [18] M. Ackermann et al. Resolving the Extragalactic γ -Ray Background above 50 GeV with the Fermi Large Area Telescope. *Phys. Rev. Lett.*, 116(15):151105, 2016. doi: 10.1103/PhysRevLett.116.151105.
 - [19] Mariangela Lisanti, Siddharth Mishra-Sharma, Lina Necib, and Benjamin R. Safdi. Deciphering Contributions to the Extragalactic Gamma-Ray Background from 2 GeV to 2 TeV. *Astrophys. J.*, 832(2):117, 2016. doi: 10.3847/0004-637X/832/2/117.
 - [20] M. Ajello et al. The Origin of the Extragalactic Gamma-Ray Background and Implications for Dark-Matter Annihilation. *Astrophys. J.*, 800(2):L27, 2015. doi: 10.1088/2041-8205/800/2/L27.
 - [21] M. Ackermann et al. Limits on Dark Matter Annihilation Signals from the Fermi LAT 4-year Measurement of the Isotropic Gamma-Ray Background. *JCAP*, 1509(09):008, 2015. doi: 10.1088/1475-7516/2015/09/008.
 - [22] Mattia Di Mauro, Alessandro Cuoco, Fiorenza Donato, and Jennifer M. Siegal-Gaskins. Fermi-LAT γ -ray anisotropy and intensity explained by unresolved Radio-Loud Active Galactic Nuclei. *JCAP*, 1411(11):

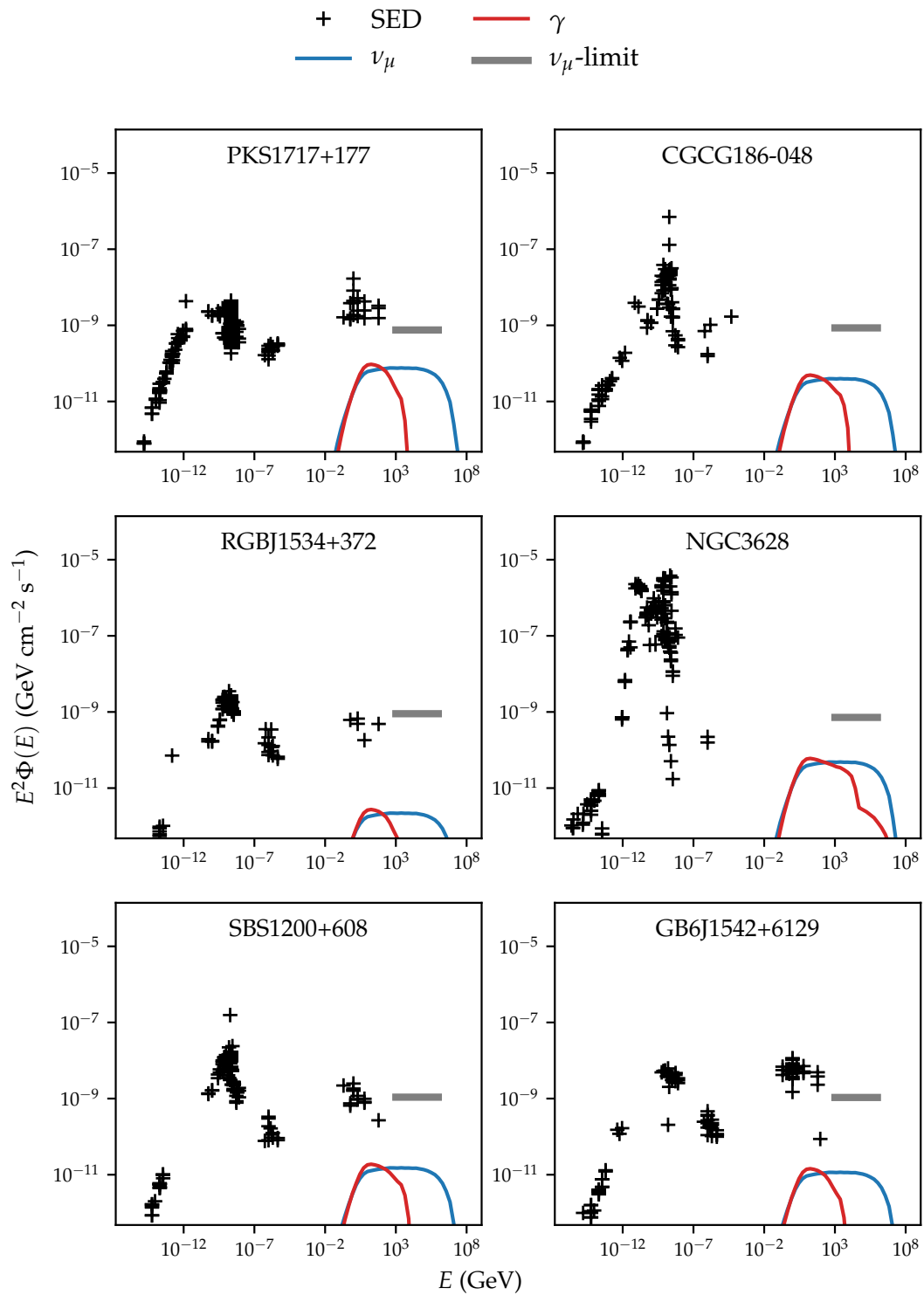


FIG. 8: Hybrid SED for all the objects in the selection besides 3C371, similar to Figure 2 for 3C371. Limit on the muon neutrino flux from [7]. Electromagnetic data (citations in Table IV) retrieved using the SSDC SED Builder [122].

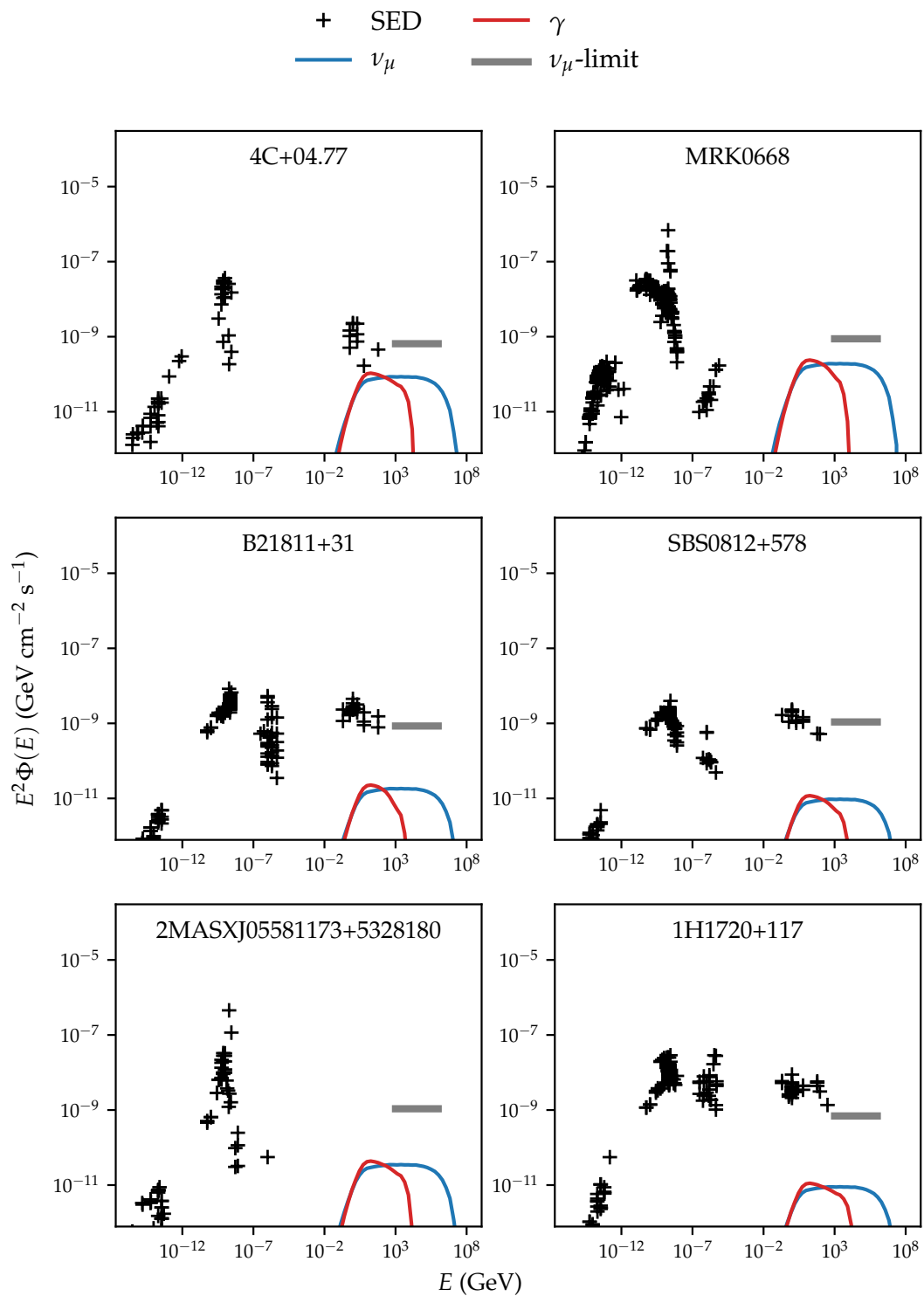


FIG. 9: Hybrid SED for all the other objects in the selection, continued.

TABLE IV: Citations for the electromagnetic data used in Figures 8, 9 and 10.

Object	Citations
PKS1717+177	[96–98, 100, 101, 104–108, 110–113, 115, 116, 118–121, 157, 158]
CGCG186-048	[96–98, 101, 105, 106, 110, 111, 115–117, 157, 159]
RGBJ1534+372	[96, 100, 101, 105, 110, 112, 113, 115–117, 119–121, 157, 159]
NGC3628	[96, 97, 101–108, 159]
SBS1200+608	[96, 97, 101, 105, 106, 110–113, 115, 116, 118–121, 157, 159]
GB6J1542+6129	[96, 97, 101, 105, 106, 108, 112, 113, 115, 116, 118–121, 159]
4C+04.77	[98, 107, 118–120]
MRK0668	[96–99, 101–103, 105, 106, 110–113, 157, 159, 160]
3C371	[95–121]
B21811+31	[96–98, 100, 101, 105, 106, 110, 112, 113, 115, 116, 118–121, 157]
SBS0812+578	[96, 101, 105, 110–113, 115, 116, 118–121, 159]
2MASXJ05581173+5328180	[96, 97, 100, 101, 105, 106, 110, 111, 157]
1H1720+117	[96, 97, 100, 101, 105, 110–113, 115–121, 157, 161, 162]
ARP220	[96, 97, 101–108, 110, 157, 159, 160]

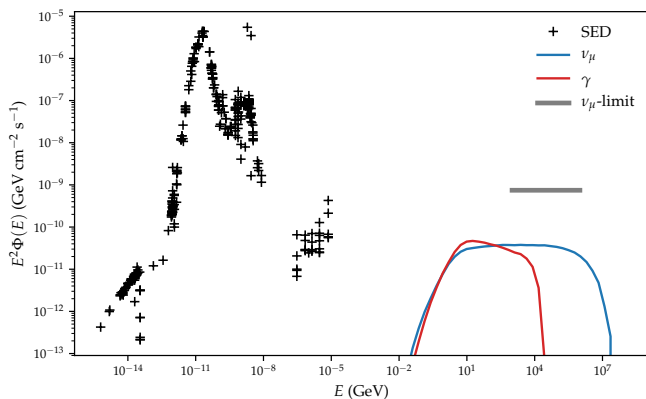


FIG. 10: Hybrid SED for ARP 220. Note the different scale.

- 021, 2014. doi: 10.1088/1475-7516/2014/11/021.
- [23] Yoshiyuki Inoue. Cosmic Gamma-ray Background Radiation. In *5th International Fermi Symposium Nagoya, Japan, October 20-24, 2014*, 2014. URL <https://inspirehep.net/record/1334100/files/arXiv:1412.3886.pdf>.
- [24] Luigi Costamante. Gamma-rays from Blazars and the Extragalactic Background Light. *Int. J. Mod. Phys.*, D22(13):1330025, 2013. doi: 10.1142/S0218271813300255.
- [25] W. B. Atwood et al. The Large Area Telescope on the Fermi Gamma-ray Space Telescope Mission. *Astrophys. J.*, 697:1071–1102, 2009. doi: 10.1088/0004-637X/697/2/1071.
- [26] W. Atwood et al. Pass 8: Toward the Full Realization of the Fermi-LAT Scientific Potential. 2013. URL <https://inspirehep.net/record/1223837/files/arXiv:1303.3514.pdf>.
- [27] Andrea Palladino, Anatoli Fedynitch, Rasmus W. Rasmussen, and Andrew M. Taylor. IceCube Neutrinos from Hadronically Powered Gamma-Ray Galaxies. 2018.
- [28] Kohta Murase, Dafne Guetta, and Markus Ahlers. Hidden Cosmic-Ray Accelerators as an Origin of TeV-PeV Cosmic Neutrinos. *Phys. Rev. Lett.*, 116(7):071101, 2016. doi: 10.1103/PhysRevLett.116.071101.
- [29] G. Maggi, S. Buitink, P. Correa, K. D. de Vries, G. Gentile, J. León Tavares, O. Scholten, N. van Eijndhoven, M. Vereecken, and T. Winchen. Obscured flat spectrum radio active galactic nuclei as sources of high-energy neutrinos. *Phys. Rev.*, D94(10):103007, 2016. doi: 10.1103/PhysRevD.94.103007.
- [30] H. Bethe and W. Heitler. On the Stopping of fast particles and on the creation of positive electrons. *Proc. Roy. Soc. Lond.*, A146:83–112, 1934. doi: 10.1098/rspa.1934.0140.
- [31] S. R. Kelner, Felex A. Aharonian, and V. V. Bugayov. Energy spectra of gamma-rays, electrons and neutrinos produced at proton-proton interactions in the very high energy regime. *Phys. Rev.*, D74:034018, 2006. doi: 10.1103/PhysRevD.74.034018, 10.1103/PhysRevD.79.039901. [Erratum: *Phys. Rev. D*79,039901(2009)].
- [32] Lukas Nellen, Karl Mannheim, and Peter L. Biermann. Neutrino production through hadronic cascades in AGN accretion disks. *Phys. Rev.*, D47:5270–5274, 1993. doi: 10.1103/PhysRevD.47.5270.
- [33] J. Becker Tjus, B. Eichmann, F. Halzen, A. Kheirandish, and S. M. Saba. High-energy neutrinos from radio galaxies. *Phys. Rev.*, D89(12):123005, 2014. doi: 10.1103/PhysRevD.89.123005.
- [34] Matias M. Reynoso, Hugo R. Christiansen, and Gustavo E. Romero. Gamma-ray absorption in the microquasar SS433. *Astropart. Phys.*, 28:565–572, 2008. doi: 10.1016/j.astropartphys.2007.10.005.
- [35] Matias M. Reynoso, Gustavo E. Romero, and Hugo R. Christiansen. Production of gamma rays and neutrinos in the dark jets of the microquasar SS433. *Mon. Not. Roy. Astron. Soc.*, 387:1745–1754, 2008. doi: 10.1111/j.1365-2966.2008.13364.x.
- [36] Matías M. Reynoso and Agustín M. Carulli. On the possibilities of high-energy neutrino production in the jets of microquasar SS433 in light of new observational data. *Astropart. Phys.*, 109:25–32, 2019. doi: 10.1016/j.astropartphys.2019.02.003.
- [37] J. M. Pittard, T. W. Hartquist, and S. A. E. G. Falle. The turbulent destruction of clouds - II. Mach number dependence, mass-loss rates and tail formation. *MNRAS*, 405(2):821–838, Jun 2010. doi: 10.1111/j.1365-2966.2010.16504.x.

- [38] A. T. Araudo, V. Bosch-Ramon, and G. E. Romero. Gamma rays from cloud penetration at the base of AGN jets. *A&A*, 522:A97, November 2010. doi: 10.1051/0004-6361/201014660.
- [39] Arnon Dar and Ari Laor. Hadronic production of TeV gamma-ray flares from blazars. *Astrophys. J.*, 478:L5–L8, 1997. doi: 10.1086/310544.
- [40] Nicholas Senno, Kohta Murase, and Peter Meszaros. Choked Jets and Low-Luminosity Gamma-Ray Bursts as Hidden Neutrino Sources. *Phys. Rev.*, D93(8):083003, 2016. doi: 10.1103/PhysRevD.93.083003.
- [41] Ruo-Yu Liu, Kai Wang, Rui Xue, Andrew M. Taylor, Xiang-Yu Wang, Zhuo Li, and Huirong Yan. A hadronuclear interpretation of a high-energy neutrino event coincident with a blazar flare. 2018.
- [42] Maxim V. Barkov, Valentí Bosch-Ramon, and Felix A. Aharonian. Interpretation of the Flares of M87 at TeV Energies in the Cloud-Jet Interaction Scenario. *ApJ*, 755(2):170, Aug 2012. doi: 10.1088/0004-637X/755/2/170.
- [43] Kai Wang, Ruo-Yu Liu, Zhuo Li, Xiang-Yu Wang, and Zi-Gao Dai. Jet-cloud/star interaction as an interpretation of neutrino outburst from the blazar TXS 0506+056. 2018.
- [44] S. del Palacio, V. Bosch-Ramon, and G. E. Romero. Gamma rays from jets interacting with BLR clouds in blazars. *Astron. Astrophys.*, 623:A101, 2019. doi: 10.1051/0004-6361/201834231.
- [45] D. V. Khangulyan, M. V. Barkov, V. Bosch-Ramon, F. A. Aharonian, and A. V. Dorodnitsyn. Star-Jet Interactions and Gamma-Ray Outbursts from 3C454.3. *Astrophys. J.*, 774:113, 2013. doi: 10.1088/0004-637X/774/2/113.
- [46] P. Banasiński, W. Bednarek, and J. Sitarek. Orphan γ -ray flares from relativistic blobs encountering luminous stars. *Mon. Not. Roy. Astron. Soc.*, 463(1):L26–L30, 2016. doi: 10.1093/mnras/slw149.
- [47] Stefano Bianchi, Roberto Maiolino, and Guido Risaliti. AGN Obscuration and the Unified Model. *Adv. Astron.*, 2012:782030, 2012. doi: 10.1155/2012/782030.
- [48] Cristina Ramos Almeida and Claudio Ricci. Nuclear obscuration in active galactic nuclei. *Nature Astronomy*, 1:679–689, Oct 2017. doi: 10.1038/s41550-017-0232-z.
- [49] Andrea Comastri. Compton thick AGN: The Dark side of the x-ray background. *Astrophys. Space Sci. Libr.*, 308:245, 2004. doi: 10.1007/978-1-4020-2471-9_8.
- [50] C. Ricci, Y. Ueda, M. J. Koss, B. Trakhtenbrot, F. E. Bauer, and P. Gandhi. Compton-thick Accretion in the local Universe. *Astrophys. J.*, 815:L13, 2015. doi: 10.1088/2041-8205/815/1/L13.
- [51] Martin C. Weisskopf, Harvey D. Tananbaum, Leon P. Van Speybroeck, and Stephen L. O’Dell. Chandra X-ray Observatory (CXO): overview. In Joachim E. Truemper and Bernd Aschenbach, editors, *X-Ray Optics, Instruments, and Missions III*, volume 4012 of *Society of Photo-Optical Instrumentation Engineers (SPIE) Conference Series*, pages 2–16, Jul 2000. doi: 10.1117/12.391545.
- [52] Junyao Li et al. Piercing Through Highly Obscured and Compton-thick AGNs in the Chandra Deep Fields: I. X-ray Spectral and Long-term Variability Analyses. 2019.
- [53] G. Risaliti, R. Maiolino, and M. Salvati. The Distribution of absorbing column densities among seyfert 2 galaxies. *Astrophys. J.*, 522:157–164, 1999. doi: 10.1086/307623.
- [54] Murray Brightman, Kirpal Nandra, Mara Salvato, Li-Ting Hsu, Cyprian Rangel, and James Aird. Compton thick active galactic nuclei in Chandra surveys. *Mon. Not. Roy. Astron. Soc.*, 443(3):1999–2017, 2014. doi: 10.1093/mnras/stu1175.
- [55] I. García-Bernete, C. Ramos Almeida, A. Alonso-Herrero, M. J. Ward, J. A. Acosta-Pulido, M. Pereira-Santaella, A. Hernán-Caballero, A. Asensio Ramos, O. González-Martín, N. A. Levenson, S. Mateos, F. J. Carrera, C. Ricci, P. Roche, I. Marquez, C. Packham, J. Masegosa, and L. Fuller. Torus model properties of an ultra-hard X-ray selected sample of Seyfert galaxies. *arXiv e-prints*, art. arXiv:1904.03694, Apr 2019.
- [56] Hans A. Krimm et al. The Swift/BAT Hard X-ray Transient Monitor. *Astrophys. J. Suppl.*, 209:14, 2013. doi: 10.1088/0067-0049/209/1/14.
- [57] Michael J. Koss, R. Assef, M. Baloković, D. Stern, P. Gandhi, I. Lamperti, D. M. Alexander, D. R. Ballantyne, F. E. Bauer, S. Berney, W. N. Brandt, A. Comastri, N. Gehrels, F. A. Harrison, G. Lansbury, C. Markwardt, C. Ricci, E. Rivers, K. Schawinski, B. Trakhtenbrot, E. Treister, and C. Megan Urry. A New Population of Compton-thick AGNs Identified Using the Spectral Curvature above 10 keV. *ApJ*, 825(2):85, Jul 2016. doi: 10.3847/0004-637X/825/2/85.
- [58] S. Mateos, F. J. Carrera, X. Barcons, A. Alonso-Herrero, A. Hernán-Caballero, M. Page, C. Ramos Almeida, A. Caccianiga, T. Miyaji, and A. Blain. Survival of the obscuring torus in the most powerful active galactic nuclei. *Astrophys. J.*, 841(2):L18, 2017. doi: 10.3847/2041-8213/aa7268.
- [59] P. F. Roche, A. Alonso-Herrero, and O. Gonzalez-Martin. The silicate absorption profile in the interstellar medium towards the heavily obscured nucleus of NGC 4418. *MNRAS*, 449(3):2598–2603, May 2015. doi: 10.1093/mnras/stv495.
- [60] Kazushi Sakamoto, Susanne Aalto, Francesco Costagliola, Sergio Martin, Youichi Ohyama, Martina C. Wiedner, and David J. Wilner. Submillimeter Interferometry of the Luminous Infrared Galaxy NGC 4418: A Hidden Hot Nucleus with an Inflow and an Outflow. *Astrophys. J.*, 764:42, 2013. doi: 10.1088/0004-637X/764/1/42.
- [61] F. Costagliola, S. Aalto, K. Sakamoto, S. Martín, R. Beswick, S. Muller, and H. R. Klöckner. A high-resolution mm and cm study of the obscured LIRG NGC 4418 - A compact obscured nucleus fed by infalling gas? *Astron. Astrophys.*, 556:A66, 2013. doi: 10.1051/0004-6361/201220634.
- [62] A. Lawrence and M. Elvis. Misaligned Discs as Obscurers in Active Galaxies. *ArXiv e-prints*, February 2010.
- [63] K. A. Arnaud. XSPEC: The First Ten Years. In G. H. Jacoby and J. Barnes, editors, *Astronomical Data Analysis Software and Systems V*, volume 101 of *Astronomical Society of the Pacific Conference Series*, page 17, 1996.
- [64] E. Anders and N. Grevesse. Abundances of the elements: Meteoritic and solar. *Geochim. Cosmochim. Acta*, 53:197–214, 1989. doi: 10.1016/0016-7037(89)90286-X.
- [65] E. Gattuzz, J. García, T. R. Kallman, C. Mendoza, and T. W. Gorczyca. ISMabs: A Comprehensive X-Ray Absorption Model for the Interstellar Medium. *ApJ*, 800:

- 29, February 2015. doi: 10.1088/0004-637X/800/1/29.
- [66] K. Mannheim and R. Schlickeiser. Interactions of Cosmic Ray Nuclei. *Astron. Astrophys.*, 286:983–996, 1994.
- [67] M.J. Berger, J.H. Hubbell, S.M. Seltzer, J. Chang, J.S. Coursey, R. Sukumar, D.S. Zucker, and K. Olsen. XCOM: Photon Cross Section Database (version 1.5) [online], 2010. URL <http://physics.nist.gov/xcom>. National Institute of Standards and Technology, Gaithersburg, MD.
- [68] M. J. Chodorowski, A. A. Zdziarski, and M. Sikora. Reaction rate and energy-loss rate for photopair production by relativistic nuclei. *ApJ*, 400:181–185, November 1992. doi: 10.1086/171984.
- [69] R. Ruffini, G. V. Vereshchagin, and S. S. Xue. Cosmic absorption of ultra high energy particles. *Astrophys. Space Sci.*, 361:82, 2016. doi: 10.1007/s10509-016-2668-5.
- [70] Mitchell C. Begelman, Bronislaw Rudak, and Marek Sikora. Consequences of Relativistic Proton Injection in Active Galactic Nuclei. *ApJ*, 362:38, Oct 1990. doi: 10.1086/169241.
- [71] L. D. Landau and I. Pomeranchuk. Limits of applicability of the theory of bremsstrahlung electrons and pair production at high-energies. *Dokl. Akad. Nauk Ser. Fiz.*, 92:535–536, 1953.
- [72] L. D. Landau and I. Pomeranchuk. Electron cascade process at very high-energies. *Dokl. Akad. Nauk Ser. Fiz.*, 92:735–738, 1953.
- [73] Arkady B. Migdal. Bremsstrahlung and pair production in condensed media at high-energies. *Phys. Rev.*, 103:1811–1820, 1956. doi: 10.1103/PhysRev.103.1811.
- [74] D.T. Haar. *Collected Papers of L.D. Landau*. Elsevier Science, 2013. ISBN 9781483152707. URL <https://books.google.be/books?id=epc4BQAAQBAJ>.
- [75] Spencer Klein. Suppression of Bremsstrahlung and pair production due to environmental factors. *Rev. Mod. Phys.*, 71:1501–1538, 1999. doi: 10.1103/RevModPhys.71.1501.
- [76] M. Tanabashi et al. Review of Particle Physics. *Phys. Rev.*, D98(3):030001, 2018. doi: 10.1103/PhysRevD.98.030001.
- [77] Charles D. Dermer, Kohta Murase, and Hajime Takami. Variable Gamma-Ray Emission Induced by Ultra-high Energy Neutral Beams: Application to 4C +21.35. *ApJ*, 755(2):147, Aug 2012. doi: 10.1088/0004-637X/755/2/147.
- [78] S. Hummer, M. Maltoni, W. Winter, and C. Yaguna. Energy dependent neutrino flavor ratios from cosmic accelerators on the Hillas plot. *Astropart. Phys.*, 34:205–224, 2010. doi: 10.1016/j.astropartphys.2010.07.003.
- [79] S. P. O’Sullivan and D. C. Gabuzda. Magnetic field strength and spectral distribution of six parsec-scale active galactic nuclei jets. *MNRAS*, 400(1):26–42, Nov 2009. doi: 10.1111/j.1365-2966.2009.15428.x.
- [80] Eli Waxman and John N. Bahcall. High-energy neutrinos from cosmological gamma-ray burst fireballs. *Phys. Rev. Lett.*, 78:2292–2295, 1997. doi: 10.1103/PhysRevLett.78.2292.
- [81] P. Padovani and C. M. Urry. Luminosity Functions, Relativistic Beaming, and Unified Theories of High-Luminosity Radio Sources. *ApJ*, 387:449, March 1992. doi: 10.1086/171098.
- [82] Lukas Merten, Julia Becker Tjus, Björn Eichmann, and Ralf-Jürgen Dettmar. On the non-thermal electron-to-proton ratio at cosmic ray acceleration sites. *Astropart. Phys.*, 90:75–84, 2017. doi: 10.1016/j.astropartphys.2017.02.007.
- [83] R. S. Fletcher, T. K. Gaisser, Paolo Lipari, and Todor Stanev. SIBYLL: An Event generator for simulation of high-energy cosmic ray cascades. *Phys. Rev.*, D50:5710–5731, 1994. doi: 10.1103/PhysRevD.50.5710.
- [84] N.N. Kalmykov, S.S. Ostapchenko, and A.I. Pavlov. Quark-gluon-string model and eas simulation problems at ultra-high energies. *Nuclear Physics B - Proceedings Supplements*, 52(3):17 – 28, 1997. ISSN 0920-5632. doi: [https://doi.org/10.1016/S0920-5632\(96\)00846-8](https://doi.org/10.1016/S0920-5632(96)00846-8). URL <http://www.sciencedirect.com/science/article/pii/S0920563296008468>.
- [85] Eun-Joo Ahn, Ralph Engel, Thomas K. Gaisser, Paolo Lipari, and Todor Stanev. Cosmic ray interaction event generator SIBYLL 2.1. *Phys. Rev.*, D80:094003, 2009. doi: 10.1103/PhysRevD.80.094003.
- [86] Felix Riehn, Ralph Engel, Anatoli Fedynitch, Thomas K. Gaisser, and Todor Stanev. Charm production in SIBYLL. *EPJ Web Conf.*, 99:12001, 2015. doi: 10.1051/epjconf/20159912001.
- [87] Felix Riehn, Ralph Engel, Anatoli Fedynitch, Thomas K. Gaisser, and Todor Stanev. A new version of the event generator Sibyll. *PoS, ICRC2015*: 558, 2016. doi: 10.22323/1.236.0558.
- [88] S. Agostinelli et al. GEANT4: A Simulation toolkit. *Nucl. Instrum. Meth.*, A506:250–303, 2003. doi: 10.1016/S0168-9002(03)01368-8.
- [89] Torbjörn Sjöstrand, Stefan Ask, Jesper R. Christiansen, Richard Corke, Nishita Desai, Philip Ilten, Stephen Mrenna, Stefan Prestel, Christine O. Rasmussen, and Peter Z. Skands. An Introduction to PYTHIA 8.2. *Comput. Phys. Commun.*, 191:159–177, 2015. doi: 10.1016/j.cpc.2015.01.024.
- [90] G. Ghisellini, F. Tavecchio, L. Foschini, G. Ghirlanda, L. Maraschi, and A. Celotti. General physical properties of bright Fermi blazars. *MNRAS*, 402:497–518, February 2010. doi: 10.1111/j.1365-2966.2009.15898.x.
- [91] V. Beckmann and C. Shrader. *Active Galactic Nuclei*. Physics textbook. Wiley, 2012. ISBN 9783527410910. URL <https://books.google.be/books?id=c44yvicEX70C>.
- [92] R. Schlickeiser. *Cosmic Ray Astrophysics*. Astronomy and Astrophysics Library. Springer Berlin Heidelberg, 2014. ISBN 9783662048153. URL <https://books.google.be/books?id=1K8PswEACAAJ>.
- [93] Yoshiyuki Inoue, Susumu Inoue, Masakazu A. R. Kobayashi, Ryu Makiya, Yuu Niino, and Tomonori Totani. Extragalactic Background Light from Hierarchical Galaxy Formation: Gamma-ray Attenuation up to the Epoch of Cosmic Reionization and the First Stars. *Astrophys. J.*, 768:197, 2013. doi: 10.1088/0004-637X/768/2/197.
- [94] M. G. Aartsen et al. Neutrino astronomy with the next generation IceCube Neutrino Observatory. 2019.
- [95] P. Giommi, M. Capalbi, M. Focchi, E. Memola, M. Perri, S. Piranomonte, S. Rebecchi, and E. Massaro. A Catalog of 157 X-ray Spectra and 84 Spectral Energy Distributions of Blazars Observed with BeppoSAX. In P. Giommi, E. Massaro, and G. Palumbo, editors, *Blazar Astrophysics with BeppoSAX and Other Observatories*, page 63, 2002.
- [96] S. T. Myers, N. J. Jackson, I. W. A. Browne, A. G.

- de Bruyn, T. J. Pearson, A. C. S. Readhead, P. N. Wilkinson, A. D. Biggs, R. D. Blandford, C. D. Fassnacht, L. V. E. Koopmans, D. R. Marlow, J. P. McKean, M. A. Norbury, P. M. Phillips, D. Rusin, M. C. Shepherd, and C. M. Sykes. The Cosmic Lens All-Sky Survey - I. Source selection and observations. *MNRAS*, 341:1–12, May 2003. doi: 10.1046/j.1365-8711.2003.06256.x.
- [97] S. E. Healey, R. W. Romani, G. B. Taylor, E. M. Sadler, R. Ricci, T. Murphy, J. S. Ulvestad, and J. N. Winn. CRATES: An All-Sky Survey of Flat-Spectrum Radio Sources. *ApJS*, 171:61–71, July 2007. doi: 10.1086/513742.
- [98] R. S. Dixon. A Master List of Radio Sources. *ApJS*, 20:1–503, July 1970. doi: 10.1086/190216.
- [99] H. Kuehr, A. Witzel, I. I. K. Pauliny-Toth, and U. Nauber. A catalogue of extragalactic radio sources having flux densities greater than 1 Jy at 5 GHz. *A&AS*, 45:367–430, September 1981.
- [100] E. Nieppola, M. Tornikoski, A. Lähteenmäki, E. Valtaoja, T. Hakala, T. Hovatta, M. Kotiranta, S. Nummila, T. Ojala, M. Parviainen, M. Ranta, P.-M. Saloranta, I. Tornainen, and M. Tröller. 37 GHz Observations of a Large Sample of BL Lacertae Objects. *AJ*, 133:1947–1953, May 2007. doi: 10.1086/512609.
- [101] J. J. Condon, W. D. Cotton, E. W. Greisen, Q. F. Yin, R. A. Perley, G. B. Taylor, and J. J. Broderick. The NRAO VLA Sky Survey. *AJ*, 115:1693–1716, May 1998. doi: 10.1086/300337.
- [102] M. Moshir and et al. IRAS Faint Source Catalogue, version 2.0. In *IRAS Faint Source Catalogue, version 2.0 (1990)*, page 0, 1990.
- [103] W. G. Joint Iras Science. VizieR Online Data Catalog: IRAS catalogue of Point Sources, Version 2.0 (IPAC 1986). *VizieR Online Data Catalog*, 2125:0, January 1994.
- [104] Planck Collaboration, P. A. R. Ade, N. Aghanim, M. Arnaud, M. Ashdown, J. Aumont, C. Baccigalupi, A. Balbi, A. J. Banday, R. B. Barreiro, and et al. Planck early results. VII. The Early Release Compact Source Catalogue. *A&A*, 536:A7, December 2011. doi: 10.1051/0004-6361/201116474.
- [105] P. C. Gregory, W. K. Scott, K. Douglas, and J. J. Condon. The GB6 Catalog of Radio Sources. *ApJS*, 103:427, April 1996. doi: 10.1086/192282.
- [106] R. L. White and R. H. Becker. A new catalog of 30,239 1.4 GHz sources. *ApJS*, 79:331–467, April 1992. doi: 10.1086/191656.
- [107] Planck Collaboration, P. A. R. Ade, N. Aghanim, F. Argüeso, C. Armitage-Caplan, M. Arnaud, M. Ashdown, F. Atrio-Barandela, J. Aumont, C. Baccigalupi, and et al. Planck 2013 results. XXVIII. The Planck Catalogue of Compact Sources. *A&A*, 571:A28, November 2014. doi: 10.1051/0004-6361/201321524.
- [108] Planck Collaboration, P. A. R. Ade, N. Aghanim, F. Argüeso, M. Arnaud, M. Ashdown, J. Aumont, C. Baccigalupi, A. J. Banday, R. B. Barreiro, and et al. Planck 2015 results. XXVI. The Second Planck Catalogue of Compact Sources. *ArXiv e-prints*, July 2015.
- [109] E. L. Wright, X. Chen, N. Odegard, C. L. Bennett, R. S. Hill, G. Hinshaw, N. Jarosik, E. Komatsu, M. R. Nolte, L. Page, D. N. Spergel, J. L. Weiland, E. Wollack, J. Dunkley, B. Gold, M. Halpern, A. Kogut, D. Larson, M. Limon, S. S. Meyer, and G. S. Tucker. Five-Year Wilkinson Microwave Anisotropy Probe Observations: Source Catalog. *ApJS*, 180:283–295, February 2009. doi: 10.1088/0067-0049/180/2/283.
- [110] E. L. Wright, P. R. M. Eisenhardt, A. K. Mainzer, M. E. Ressler, R. M. Cutri, T. Jarrett, J. D. Kirkpatrick, D. Padgett, R. S. McMillan, M. Skrutskie, S. A. Stanford, M. Cohen, R. G. Walker, J. C. Mather, D. Leisawitz, T. N. Gautier, III, I. McLean, D. Benford, C. J. Lonsdale, A. Blain, B. Mendez, W. R. Irace, V. Duval, F. Liu, D. Royer, I. Heinrichsen, J. Howard, M. Shannon, M. Kendall, A. L. Walsh, M. Larsen, J. G. Cardon, S. Schick, M. Schwalm, M. Abid, B. Fabinsky, L. Naes, and C.-W. Tsai. The Wide-field Infrared Survey Explorer (WISE): Mission Description and Initial On-orbit Performance. *AJ*, 140:1868, December 2010. doi: 10.1088/0004-6256/140/6/1868.
- [111] L. Bianchi, B. Efremova, J. Herald, L. Girardi, A. Zabot, P. Marigo, and C. Martin. Catalogues of hot white dwarfs in the Milky Way from GALEX’s ultraviolet sky surveys: constraining stellar evolution. *MNRAS*, 411:2770–2791, March 2011. doi: 10.1111/j.1365-2966.2010.17890.x.
- [112] V. D’Elia, M. Perri, S. Puccetti, M. Capalbi, P. Giommi, D. N. Burrows, S. Campana, G. Tagliaferri, G. Cusumano, P. Evans, N. Gehrels, J. Kennea, A. Moretti, J. A. Nousek, J. P. Osborne, P. Romano, and G. Stratta. The seven year Swift-XRT point source catalog (1SWXRT). *A&A*, 551:A142, March 2013. doi: 10.1051/0004-6361/201220863.
- [113] P. A. Evans, J. P. Osborne, A. P. Beardmore, K. L. Page, R. Willingale, C. J. Mountford, C. Pagani, D. N. Burrows, J. A. Kennea, M. Perri, G. Tagliaferri, and N. Gehrels. 1sxs: A deep swift x-ray telescope point source catalog with light curves and spectra. *The Astrophysical Journal Supplement Series*, 210(1):8, 2014. URL <http://stacks.iop.org/0067-0049/210/i=1/a=8>.
- [114] M. Elvis, D. Plummer, J. Schachter, and G. Fabbiano. The Einstein Slew Survey. *ApJS*, 80:257–303, May 1992. doi: 10.1086/191665.
- [115] W. Voges, B. Aschenbach, T. Boller, H. Bräuninger, U. Briel, W. Burkert, K. Dennerl, J. Englhauser, R. Gruber, F. Haberl, G. Hartner, G. Hasinger, M. Kürster, E. Pfeffermann, W. Pietsch, P. Predehl, C. Rosso, J. H. M. M. Schmitt, J. Trümper, and H. U. Zimmermann. The ROSAT all-sky survey bright source catalogue. *A&A*, 349:389–405, September 1999.
- [116] T. Boller, M. J. Freyberg, J. Trümper, F. Haberl, W. Voges, and K. Nandra. Second ROSAT all-sky survey (2RXS) source catalogue. *aap*, 588:A103, April 2016. doi: 10.1051/0004-6361/201525648.
- [117] R. D. Saxton, A. M. Read, P. Esquej, M. J. Freyberg, B. Altieri, and D. Bermejo. The first XMM-Newton slew survey catalogue: XMMSL1. *A&A*, 480:611–622, March 2008. doi: 10.1051/0004-6361:20079193.
- [118] A. A. Abdo, M. Ackermann, M. Ajello, A. Allafort, E. Antolini, W. B. Atwood, M. Axelsson, L. Baldini, J. Ballet, G. Barbiellini, and et al. Fermi Large Area Telescope First Source Catalog. *ApJS*, 188:405–436, June 2010. doi: 10.1088/0067-0049/188/2/405.
- [119] P. L. Nolan, A. A. Abdo, M. Ackermann, M. Ajello, A. Allafort, E. Antolini, W. B. Atwood, M. Axelsson, L. Baldini, J. Ballet, and et al. Fermi Large Area Telescope Second Source Catalog. *ApJS*, 199:31, April 2012. doi: 10.1088/0067-0049/199/2/31.

- [120] F. Acero, M. Ackermann, M. Ajello, A. Albert, W. B. Atwood, M. Axelsson, L. Baldini, J. Ballet, G. Barbiellini, D. Bastieri, A. Belfiore, R. Bellazzini, E. Bissaldi, R. D. Blandford, E. D. Bloom, J. R. Bogart, R. Bonino, E. Bottacini, J. Bregeon, R. J. Britto, P. Bruel, R. Buehler, T. H. Burnett, S. Buson, G. A. Calianandro, R. A. Cameron, R. Caputo, M. Caragiulo, P. A. Caraveo, J. M. Casandjian, E. Cavazzuti, E. Charles, R. C. G. Chaves, A. Chekhtman, C. C. Cheung, J. Chiang, G. Chiaro, S. Ciprini, R. Claus, J. Cohen-Tanugi, L. R. Cominsky, J. Conrad, S. Cutini, F. D’Ammando, A. de Angelis, M. DeKlotz, F. de Palma, R. Desiante, S. W. Digel, L. Di Venere, P. S. Drell, R. Dubois, D. Dumora, C. Favuzzi, S. J. Fegan, E. C. Ferrara, J. Finke, A. Franckowiak, Y. Fukazawa, S. Funk, P. Fusco, F. Gargano, D. Gasparrini, B. Giebels, N. Giglietto, P. Giommi, F. Giordano, M. Giroletti, T. Glanzman, G. Godfrey, I. A. Grenier, M.-H. Grondin, J. E. Grove, L. Guillemot, S. Guiriec, D. Hadasch, A. K. Harding, E. Hays, J. W. Hewitt, A. B. Hill, D. Horan, G. Iafate, T. Jogler, G. Jóhannesson, R. P. Johnson, A. S. Johnson, T. J. Johnson, W. N. Johnson, T. Kamae, J. Kataoka, J. Katsuta, M. Kuss, G. La Mura, D. Landriu, S. Larsson, L. Latronico, M. Lemoine-Goumard, J. Li, L. Li, F. Longo, F. Loparco, B. Lott, M. N. Lovellette, P. Lubrano, G. M. Madejski, F. Massaro, M. Mayer, M. N. Mazziotta, J. E. McEnery, P. F. Michelson, N. Mirabal, T. Mizuno, A. A. Moiseev, M. Mongelli, M. E. Monzani, A. Morselli, I. V. Moskalenko, S. Murgia, E. Nuss, M. Ohno, T. Ohsugi, N. Omodei, M. Orienti, E. Orlando, J. F. Ormes, D. Paneque, J. H. Panetta, J. S. Perkins, M. Pesce-Rollins, F. Piron, G. Pivato, T. A. Porter, J. L. Racusin, R. Rando, M. Razzano, S. Razzaque, A. Reimer, O. Reimer, T. Reposeur, L. S. Rochester, R. W. Romani, D. Salvetti, M. Sánchez-Conde, P. M. Saz Parkinson, A. Schulz, E. J. Siskind, D. A. Smith, F. Spada, G. Spandre, P. Spinelli, T. E. Stephens, A. W. Strong, D. J. Suson, H. Takahashi, T. Takahashi, Y. Tanaka, J. G. Thayer, J. B. Thayer, D. J. Thompson, L. Tibaldo, O. Tibolla, D. F. Torres, E. Torresi, G. Tosti, E. Troja, B. Van Klaveren, G. Vianello, B. L. Winer, K. S. Wood, M. Wood, S. Zimmer, and Fermi-LAT Collaboration. Fermi Large Area Telescope Third Source Catalog. *ApJS*, 218:23, June 2015. doi: 10.1088/0067-0049/218/2/23.
- [121] B. Bartoli, P. Bernardini, X. J. Bi, I. Bolognino, P. Branchini, A. Budano, A. K. Calabrese Melcarne, P. Camarri, Z. Cao, R. Cardarelli, S. Catalanotti, S. Z. Chen, T. L. Chen, Y. Chen, P. Creti, S. W. Cui, B. Z. Dai, A. D’Amone, Danzengluobu, I. De Mitri, B. D’Ettore Piazzoli, T. Di Girolamo, X. H. Ding, G. Di Sciascio, C. F. Feng, Zhaoyang Feng, Zhenyong Feng, Q. B. Gou, Y. Q. Guo, H. H. He, Haibing Hu, Hongbo Hu, Q. Huang, M. Iacovacci, R. Iuppa, H. Y. Jia, Labaciren, H. J. Li, J. Y. Li, X. X. Li, G. Liguori, C. Liu, C. Q. Liu, J. Liu, M. Y. Liu, H. Lu, L. L. Ma, X. H. Ma, G. Mancarella, S. M. Mari, G. Marsella, D. Martello, S. Mastroianni, P. Montini, C. C. Ning, M. Panareo, B. Panico, L. Perrone, P. Pistilli, F. Ruggieri, P. Salvini, R. Santonico, S. N. Sbrano, P. R. Shen, X. D. Sheng, F. Shi, A. Surdo, Y. H. Tan, P. Valania, S. Vernetto, C. Vigorito, B. Wang, H. Wang, C. Y. Wu, H. R. Wu, B. Xu, L. Xue, Q. Y. Yang, X. C. Yang, Z. G. Yao, A. F. Yuan, M. Zha, H. M. Zhang, Jilong Zhang, Jianli Zhang, L. Zhang, P. Zhang, X. Y. Zhang, Y. Zhang, J. Zhao, Zhaxiciren, Zhaxiangzhu, X. X. Zhou, F. R. Zhu, Q. Q. Zhu, G. Zizzi, and The ARGO-YBJ Collaboration. Tev gamma-ray survey of the northern sky using the argo-ybj detector. *The Astrophysical Journal*, 779(1):27, 2013. URL <http://stacks.iop.org/0004-637X/779/i=1/a=27>.
- [122] SSDC SED Builder. <https://tools.ssdsc.asi.it/>. Version 1.21.
- [123] Eli Waxman and John N. Bahcall. High-energy neutrinos from astrophysical sources: An Upper bound. *Phys. Rev.*, D59:023002, 1999. doi: 10.1103/PhysRevD.59.023002.
- [124] Hasan Yuksel, Matthew D. Kistler, John F. Beacom, and Andrew M. Hopkins. Revealing the High-Redshift Star Formation Rate with Gamma-Ray Bursts. *Astrophys. J.*, 683:L5–L8, 2008. doi: 10.1086/591449.
- [125] Andrew M. Hopkins and John F. Beacom. On the normalisation of the cosmic star formation history. *Astrophys. J.*, 651:142–154, 2006. doi: 10.1086/506610.
- [126] C. D. Wilson, N. Rangwala, J. Glenn, P. R. Maloney, L. Spinoglio, and M. Pereira-Santaella. Extreme Dust Disks in Arp 220 as Revealed by ALMA. *ApJ*, 789(2):L36, Jul 2014. doi: 10.1088/2041-8205/789/2/L36.
- [127] Carol Lonsdale, Duncan Farrah, and Harding Smith. Ultraluminous infrared galaxies. 2006. doi: 10.1007/3-540-30313-8.9.
- [128] D. L. Clements, L. Dunne, and S. Eales. The submillimetre properties of ultraluminous infrared galaxies. *MNRAS*, 403:274–286, March 2010. doi: 10.1111/j.1365-2966.2009.16064.x.
- [129] Neil M. Nagar, Andrew S. Wilson, Heino Falcke, Sylvain Veilleux, and Roberto Maiolino. The AGN content of ultraluminous IR galaxies: High resolution VLA imaging of the IRAS 1Jy ULIRG sample. *Astron. Astrophys.*, 409:115–122, 2003. doi: 10.1051/0004-6361:20031069.
- [130] D. Farrah, J. Afonso, A. Efsthathiou, M. Rowan-Robinson, M. Fox, and D. Clements. Starburst and agn activity in ultraluminous infrared galaxies. *Mon. Not. Roy. Astron. Soc.*, 343:585, 2003. doi: 10.1046/j.1365-8711.2003.06696.x.
- [131] L. G. Hou, X.-B. Wu, and J. L. Han. Ultra-luminous Infrared Galaxies in Sloan Digital Sky Survey Data Release 6. *ApJ*, 704:789–802, October 2009. doi: 10.1088/0004-637X/704/1/789.
- [132] D. Fadda, L. Yan, G. Lagache, A. Sajina, D. Lutz, S. Wuyts, D. T. Frayer, D. Marcillac, E. Le Floch, K. Caputi, H. W. W. Spoon, S. Veilleux, A. Blain, and G. Helou. Ultra-deep Mid-infrared Spectroscopy of Luminous Infrared Galaxies at $z \sim 1$ and $z \sim 2$. *ApJ*, 719:425–450, August 2010. doi: 10.1088/0004-637X/719/1/425.
- [133] E. Nardini, G. Risaliti, M. Salvati, E. Sani, Y. Watabe, A. Marconi, and R. Maiolino. Exploring the active galactic nucleus and starburst content of local ultraluminous infrared galaxies through 5–8 μm spectroscopy. *Monthly Notices of the Royal Astronomical Society*, 399(3):1373–1402, 2009. doi: 10.1111/j.1365-2966.2009.15357.x. URL <http://dx.doi.org/10.1111/j.1365-2966.2009.15357.x>.
- [134] F. G. Saturni, M. Mancini, E. Pezzulli, and F. Tombesi. “Zombie” or active? An alternative explanation to the properties of star-forming galaxies at high red-

- shift. *A&A*, 617:A131, October 2018. doi: 10.1051/0004-6361/201833261.
- [135] G. Kauffmann and M. G. Haehnelt. The clustering of galaxies around quasars. *MNRAS*, 332:529–535, May 2002. doi: 10.1046/j.1365-8711.2002.05278.x.
- [136] K. M. Dasyra, L. J. Tacconi, R. I. Davies, R. Genzel, D. Lutz, T. Naab, A. Burkert, S. Veilleux, and D. B. Sanders. Dynamical properties of ultraluminous infrared galaxies. i. mass ratio conditions for ulirg activity in interacting pairs. *The Astrophysical Journal*, 638(2):745, 2006. URL <http://stacks.iop.org/0004-637X/638/i=2/a=745>.
- [137] K. M. Dasyra, L. J. Tacconi, R. I. Davies, T. Naab, R. Genzel, D. Lutz, E. Sturm, A. J. Baker, S. Veilleux, D. B. Sanders, and A. Burkert. Dynamical properties of ultraluminous infrared galaxies. ii. traces of dynamical evolution and end products of local ultraluminous mergers. *The Astrophysical Journal*, 651(2):835, 2006. URL <http://stacks.iop.org/0004-637X/651/i=2/a=835>.
- [138] Philip F. Hopkins, Lars Hernquist, Paul Martini, Thomas J. Cox, Brant Robertson, Tiziana Di Matteo, and Volker Springel. A physical model for the origin of quasar lifetimes. *The Astrophysical Journal Letters*, 625(2):L71, 2005. URL <http://stacks.iop.org/1538-4357/625/i=2/a=L71>.
- [139] Philip F. Hopkins, Lars Hernquist, Thomas J. Cox, Tiziana Di Matteo, Brant Robertson, and Volker Springel. A Unified, merger-driven model for the origin of starbursts, quasars, the cosmic x-ray background, supermassive black holes and galaxy spheroids. *Astrophys. J. Suppl.*, 163:1–49, 2006. doi: 10.1086/499298.
- [140] Scott C. Chapman, A. W. Blain, Ian Smail, and R. J. Ivison. A Redshift survey of the submillimeter galaxy population. *Astrophys. J.*, 622:772–796, 2005. doi: 10.1086/428082.
- [141] L. L. Cowie, A. J. Barger, E. B. Fomalont, and P. Capak. The Evolution of the Ultraluminous Infrared Galaxy Population from Redshift 0 to 1.5. *ApJ*, 603:L69–L72, March 2004. doi: 10.1086/383198.
- [142] Hao-Ning He, Tao Wang, Yi-Zhong Fan, Si-Ming Liu, and Da-Ming Wei. Diffuse PeV neutrino emission from ultraluminous infrared galaxies. *Phys. Rev.*, D87(6):063011, 2013. doi: 10.1103/PhysRevD.87.063011.
- [143] M. Schmidt. The Rate of Star Formation. *ApJ*, 129:243, March 1959. doi: 10.1086/146614.
- [144] R. C. Kennicutt, Jr. The star formation law in galactic disks. *ApJ*, 344:685–703, September 1989. doi: 10.1086/167834.
- [145] R. C. Kennicutt, Jr. The Global Schmidt Law in Star-forming Galaxies. *ApJ*, 498:541–552, May 1998. doi: 10.1086/305588.
- [146] M. T. Sargent, E. Schinnerer, E. Murphy, C. L. Carilli, G. Helou, H. Aussel, E. Le Floch, D. T. Frayer, O. Ilbert, P. Oesch, M. Salvato, V. Smolčić, J. Kartaltepe, and D. B. Sanders. No Evolution in the IR-Radio Relation for IR-luminous Galaxies at $z < 2$ in the COSMOS Field. *ApJ*, 714:L190–L195, May 2010. doi: 10.1088/2041-8205/714/2/L190.
- [147] David W. Hogg. Distance measures in cosmology. 1999.
- [148] S. Weinberg. *Cosmology*. OUP Oxford, 2008. ISBN 9780198526827. URL <https://books.google.be/books?id=rswTDAQAQBAJ>.
- [149] V. S. Berezhinsky and A. Yu. Smirnov. Cosmic neutrinos of ultra-high energies and detection possibility. *Astrophys. Space Sci.*, 32:461–482, 1975. doi: 10.1007/BF00643157.
- [150] Paolo S. Coppi and Felix A. Aharonian. Constraints on the VHE emissivity of the universe from the diffuse GeV gamma-ray background. *Astrophys. J.*, 487:L9–L12, 1997. doi: 10.1086/310883.
- [151] Kohta Murase. High-Energy Emission Induced by Ultra-high-Energy Photons as a Probe of Ultra-high-Energy Cosmic-Ray Accelerators Embedded in the Cosmic Web. *Astrophys. J.*, 745:L16, 2012. doi: 10.1088/2041-8205/745/2/L16.
- [152] K. Murase, C. D. Dermer, H. Takami, and G. Migliori. Blazars as Ultra-high-energy Cosmic-ray Sources: Implications for TeV Gamma-Ray Observations. *ApJ*, 749:63, April 2012. doi: 10.1088/0004-637X/749/1/63.
- [153] Kohta Murase and John F. Beacom. Constraining Very Heavy Dark Matter Using Diffuse Backgrounds of Neutrinos and Cascaded Gamma Rays. *JCAP*, 1210:043, 2012. doi: 10.1088/1475-7516/2012/10/043.
- [154] Rafael Alves Batista, Andrej Dundovic, Martin Erdmann, Karl-Heinz Kampert, Daniel Kuempel, Gero Müller, Guenter Sigl, Arjen van Vliet, David Walz, and Tobias Winchen. CRPropa 3 - a Public Astrophysical Simulation Framework for Propagating Extraterrestrial Ultra-High Energy Particles. *JCAP*, 1605(05):038, 2016. doi: 10.1088/1475-7516/2016/05/038.
- [155] Sangjin Lee. On the propagation of extragalactic high-energy cosmic and gamma-rays. *Phys. Rev.*, D58:043004, 1998. doi: 10.1103/PhysRevD.58.043004.
- [156] M. Ackermann et al. The spectrum of isotropic diffuse gamma-ray emission between 100 MeV and 820 GeV. *Astrophys. J.*, 799:86, 2015. doi: 10.1088/0004-637X/799/1/86.
- [157] N. Jackson, R. A. Battye, I. W. A. Browne, S. Joshi, T. W. B. Muxlow, and P. N. Wilkinson. A survey of polarization in the JVAS/CLASS flat-spectrum radio source surveys - I. The data and catalogue production. *MNRAS*, 376:371–377, March 2007. doi: 10.1111/j.1365-2966.2007.11442.x.
- [158] A. Wright and R. Otrupcek. Parkes Catalog, 1990, Australia telescope national facility. In *PKS Catalog (1990)*, page 0, 1990.
- [159] R. L. White, R. H. Becker, D. J. Helfand, and M. D. Gregg. A Catalog of 1.4 GHz Radio Sources from the FIRST Survey. *ApJ*, 475:479–493, February 1997.
- [160] S. R. Rosen, N. A. Webb, M. G. Watson, J. Ballet, D. Barret, V. Braito, F. J. Carrera, M. T. Ceballos, M. Coriat, R. Della Ceca, G. Denkinson, P. Esquej, S. A. Farrell, M. Freyberg, F. Grisé, P. Guillout, L. Heil, D. Law-Green, G. Lamer, D. Lin, R. Martino, L. Michel, C. Motch, A. Nebot Gomez-Moran, C. G. Page, K. Page, M. Page, M. W. Pakull, J. Pye, A. Read, P. Rodriguez, M. Sakano, R. Saxton, A. Schwobe, A. E. Scott, R. Sturm, I. Traulsen, V. Yershov, and I. Zolotukhin. The XMM-Newton serendipitous survey. VII. The third XMM-Newton serendipitous source catalogue. *ArXiv e-prints*, April 2015.
- [161] W. Forman, C. Jones, L. Cominsky, P. Julien, S. Murray, G. Peters, H. Tananbaum, and R. Giacconi. The fourth Uhuru catalog of X-ray sources. *ApJS*, 38:357–412, December 1978. doi: 10.1086/190561.
- [162] F. Verrecchia, J. J. M. in’t Zand, P. Giommi, P. Santolamazza, S. Granata, J. J. Schuurmans, and L. A. Antonelli. The BeppoSAX WFC X-ray source cat-

atalogue. *A&A*, 472:705–713, September 2007. doi:
10.1051/0004-6361:20067040.